AD-A085 473 NAVAL RESEARCH LAB WASHINGTON DC F/G 8/3
OBSERVATION BY HF RADAR OF THE PHILLIPS RESONANCE MECHANISM FOR--ETC(U)
MAR 80 D B TRIZNA, R W BOGLE, J C MOORE

UNCLASSIFIED NRL-8386 SBIE-AD-E000 426 NL

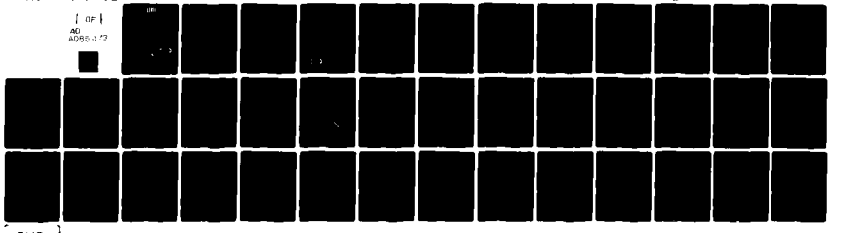

END
DATE FILMED
7-80
DTIC

NRL Report 8386

Observation by HF Radar of the Phillips Resonance Mechanism for Generation of Wind Waves

D. B. TRIZNA, R. W. BOGLE, J. C. MOORE, and C. M. HOWE

Radar Techniques Branch
Radar Division

March 14, 1980

NAVAL RESEARCH LABORATORY
Washington, D.C.

SECURITY CLASSIFICATION OF THIS PAGE (When Data Entered)

REPORT DOCUMENTATION PAGE		READ INSTRUCTIONS BEFORE COMPLETING FORM
1. REPORT NUMBER NRL Report 8386	2. GOVT ACCESSION NO. AD-A085 473	3. RECIPIENT'S CATALOG NUMBER
4. TITLE (and Subtitle) OBSERVATION BY HF RADAR OF THE PHILLIPS RESONANCE MECHANISM FOR GENERATION OF WIND WAVES		5. TYPE OF REPORT & PERIOD COVERED Interim report on a continuing NRL Problem 6. PERFORMING ORG. REPORT NUMBER
7. AUTHOR(s) D. B. Trizna, R. W. Bogle, J. C. Moore, and C. M. Howe		8. CONTRACT OR GRANT NUMBER(s)
9. PERFORMING ORGANIZATION NAME AND ADDRESS Naval Research Laboratory Washington, DC 20735		10. PROGRAM ELEMENT, PROJECT, TASK AREA & WORK UNIT NUMBERS 61153N-21 RR021-01-41 RR0210141 53-0633-0-0
11. CONTROLLING OFFICE NAME AND ADDRESS Department of Navy Office of Naval Research Arlington, VA 22217		12. REPORT DATE March 14, 1980 13. NUMBER OF PAGES 39
14. MONITORING AGENCY NAME & ADDRESS(if different from Controlling Office)		15. SECURITY CLASS. (of this report) Unclassified 15a. DECLASSIFICATION/DOWNGRADING SCHEDULE

16. DISTRIBUTION STATEMENT (of this Report)

Approved for public release; distribution unlimited.

17. DISTRIBUTION STATEMENT (of the abstract entered in Block 20, if different from Report)

18. SUPPLEMENTARY NOTES

19. KEY WORDS (Continue on reverse side if necessary and identify by block number)

Remote sensing
Directional wave spectra
Physical oceanography

20. ABSTRACT (Continue on reverse side if necessary and identify by block number)

Measurements are reported of directional ocean wave spectra made over 80 deg of viewing angle by an HF radar, operating in the surface wave mode in an area 22.5 km north of San Clemente Island, California. Ten azimuths from 280 to 360 deg true bearing were simultaneously measured for ten wave frequencies ranging from 0.14 Hz (75-m waves) to 0.35 Hz (13-m waves). A Waverider buoy was used to measure omnidirectional energy in the region, and first-order radar Bragg lines were used to determine the spreading of wave energy with angle. Data are presented

(Continued)

DD FORM 1 JAN 73 1473 EDITION OF 1 NOV 65 IS OBSOLETE
S/N 0102-014-6601

20. ABSTRACT (Continued)

in which a bimodal spectrum was present: an attenuated spectrum with wave components to 0.10 Hz from a storm at sea at 270 deg bearing; and a transient local wind spectrum, stronger in amplitude at the higher frequencies, with wave cutoff near 0.14 Hz, and running from 315 deg bearing. Just after the onset of local winds, the westerly spectrum fit a cosine squared spread at the lowest measured frequencies. With the development of local wind which blew at a 12 to 14 knot speed for a period of 12 h, the wave spectrum spread about the wind direction as cosine thirty-second at the lowest frequencies measured, 0.14 Hz, and cosine sixty-fourth at the highest frequencies measured, 0.35 Hz. For 0.28 Hz waves, the Phillips resonance mechanism for wave generation is proposed to explain the twin peaks in amplitude observed, equally spaced either side of the wind direction. These were dominant for the earliest measurement period, and still major contributions for later measurement periods. This mechanism was found to contribute also at the higher wave frequencies, but did not dominate as it did for the 0.28 Hz waves. Coherence times are derived from the angular widths of the Phillips resonances based on predictions of Stewart and Manton and are found to agree quite well with theory. Other directional spectrum measurements are reviewed in light of these results. It is found that none had the angular resolution over the wave frequencies spanned by our radar, or did not observe the transient type of conditions which prevailed during our measurements.

CONTENTS

OBSERVATION BY HF RADAR OF THE PHILLIPS RESONANCE MECHANISM FOR GENERATION OF WIND WAVES

INTRODUCTION

Traditional oceanographic techniques of measuring the directional energy spectrum of ocean waves have typically involved in situ types of instrumentation, which requires the instruments be situated and maintained in the area of ocean one is intending to measure. These systems include various types of buoys, such as the pitch and roll buoy and the cloverleaf buoy; arrays of wave gauges at the surface of the water; and arrays of pressure sensors placed beneath the surface on the bottom which infer the instantaneous wave height based upon the pressure of the column of water directly above the gauge. Each of the different techniques has its own advantages and disadvantages, in difficulty of deployment and maintaining station, angular resolution of data, or limitations of actual areas of application. Radar techniques of measuring the ocean wave directional spectrum offer another alternative to these systems, with the primary advantage that the radar measurement need not be an in situ measurement, although it may have its own operational difficulties of a completely different nature. In any case, radar offers the oceanographer options which were not available using traditional techniques.

High-frequency radar, operating in the frequency band from 1 to 30 MHz, offers some special features not available by other radar systems. Because of the relatively low frequency used, the sea surface appears as a highly conducting surface to the radar energy and allows a surface wave mode of propagation to distances beyond the local horizon, so that extensive areas can be simultaneously measured on a continuing basis. Because it does not require aircraft or satellites to physically transport the radar to the area of interest, operational costs are typically much less for the amount of data that is gathered. If one chooses to use the skywave mode of propagation via reflection of radar energy off the ionosphere to beyond the horizon distances, the system becomes a tool for surveying truly significantly large ocean surface areas, sufficient to identify the sea structure associated with hurricanes and other large storms. Of course the quality of the data collected in this skywave propagation mode is limited to some extent, and the extraction of ocean wave parameters from such data is an area of current vigorous research.

In this work, we wish to report upon data collected in the surface wave mode of operation in an area north of San Clemente Island, Calif., using an HF radar located at the north tip of the island. The ocean patch size averaged by the radar is determined by the pulse length in the radial direction, and the antenna beamwidth in the azimuthal direction. The beam of the radar is then scanned incrementally over a total azimuthal scan of 80 deg, in steps of as high as 2 deg, the beamwidth of the antenna array at 15 MHz. The system measures the wave spectrum with a similar angular resolution which scales inversely with radar frequency. With this angular resolution and 15-km range resolution, the area of sea surface scanned can be assumed to be homogeneous. This is a good assumption for short ranges, where the scattering patches for all azimuths extend over a relatively small total area. The ocean wave parameters are determined

Manuscript submitted December 19, 1979.

from a radar measurement of first-order scattering effects in this work, the so-called Bragg line amplitudes first identified by Crombie [1]. These can be shown to be directly proportional to the spectral components of the directional wave components that satisfy the Bragg scattering relationship:

$$K_B = 2k\,, \tag{1}$$

where k is the wave number of the radar energy transmitted, and K_B is the wave number of the Bragg ocean wave spectral component. The ocean wavelength is one half the radar wavelength for the radar frequency that is used; the direction is that of the look angle of the radar. Hence, by simultaneously scanning the radar in look angle and frequency hopping through the HF band, one determines a matrix of values of the directional wave spectrum in angle and wave number. Approaching and receding components of the wave spectrum are separated by applying Doppler discrimination, just as one would do with approaching and receding targets.

The relationship between the directional wave spectrum measurement and the radar measurement is established by the radar equation:

$$P_R = \frac{P_T G^2 \lambda^2 \sigma}{(4\pi)^3 R^4 L}\,, \tag{2}$$

where

P_R is the received power referenced to the terminals of the antenna;
P_T is the power transmitted into the terminals of the antenna;
G is the power gain of the antenna array;
λ is the wavelength of the radio energy transmitted;
σ is the cross section of the target;
R is the range to the target, the center of the scattering area of the sea surface being probed; and
L is the total loss in the propagation path, primarily surface wave loss.

The cross section of the sea surface is determined by the average scattering cross section of the sea, $\sigma^o(\theta)$, and the area of the sea surface being illuminated by the radar, dA, via the equation:

$$\sigma(\theta) = \sigma^o(\theta)\, dA\,. \tag{3}$$

The area of the scattering patch in radial coordinates is given by

$$dA = c\,\Delta t\, R\, d\theta\,, \tag{4}$$

where $d\theta$ is the 3 dB beamwidth of the radar antenna, Δt is the radar pulse length, R is the range from the radar to the center of the scattering cell, and c is the speed of light.

The relation to the directional wave spectrum is then established by an equation relating the average scattering cross section of the sea and the wave spectrum [2]:

$$\sigma^o(\theta) = 4\pi K_B^4 S(K_B, \theta)\,. \tag{5}$$

Hence, a well-calibrated radar measurement where all of the parameters of Equation (2) are known can be used to determine unambiguously an ocean wave spectral component for each look angle and radar frequency one chooses to use.

In the work presented here, one of the parameters of Equation (2) was not well known, namely, an absolute value for the gain of the radar antenna. However, relative gain values as a function of steer angle were known from measurements made using a transmitter aboard a small aircraft which was flown around the antenna, while it was scanned over all twenty beam positions in a high-PRF mode. Because of the relatively slow angular speed of the aircraft, antenna patterns were traced on a single pass for all beam positions, so that relative gain measurements that were made were meaningful. These were made for several radar frequencies, and the results compared favorably with those predicted by theory [3]. Hence, theoretical values for absolute antenna gain were used in the analysis reported here. Examples of theoretical antenna patterns for the middle of three available elevation angle strings are shown in Figs. 1 through 10, running from 2 to 11 MHz radar frequency, for near zero elevation angle appropriate to surface wave propagation. Pointing direction is 39°, maximum steer angle available. There were still uncertainties in total system loss for the radar which varied with radar frequency, so that Equation (2) was still not able to be solved exactly for the radar cross section. However, the relative measurements are sufficient as long as one has a measurement of the omnidirectional sea spectrum by an independent means. This was provided by a Datawell Waverider buoy positioned by the center of the radar scattering patch which transmitted data continuously simultaneous in time with the collection of the radar data. The radar data then provided a measure of the spreading of wave energy with angle, the so-called spreading function. If one writes the directional wave spectrum as a separable product of two terms, the omnidirectional wave spectrum times a spreading function,

$$S(K, \theta) = S(K)\, F(\theta), \tag{6}$$

where the second term is normalized such that integration over angle gives unity, then the first factor is the function measured by the buoy, while the second is measured by the radar as it is steered in angle.

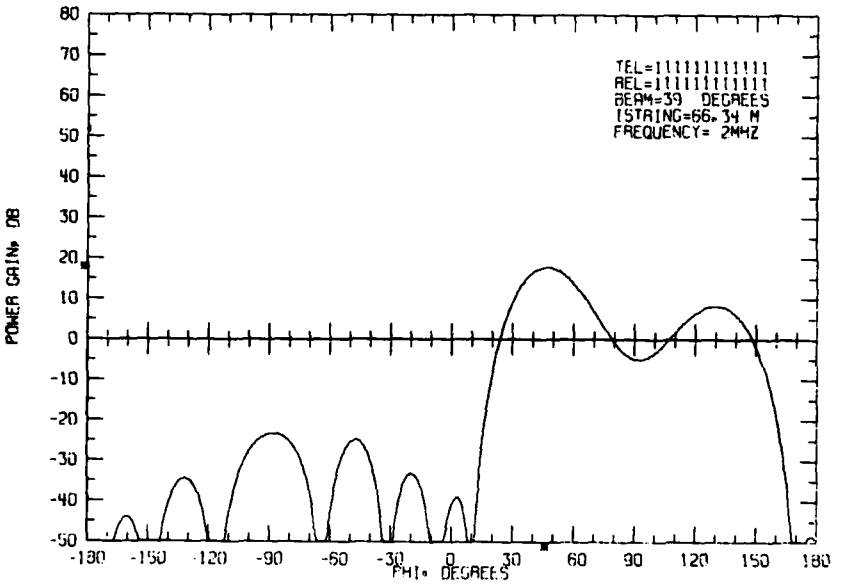

Fig. 1. Antenna pattern for 2 MHz operating frequency, mid string of three available in elevation, near zero elevation angle

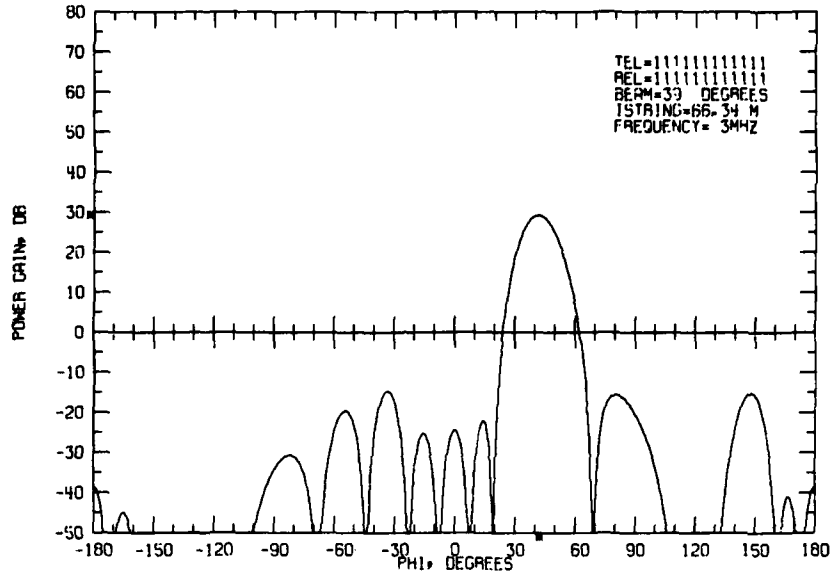

Fig. 2. Antenna pattern for 3 MHz operating frequency, mid string of three available in elevation, near zero elevation angle

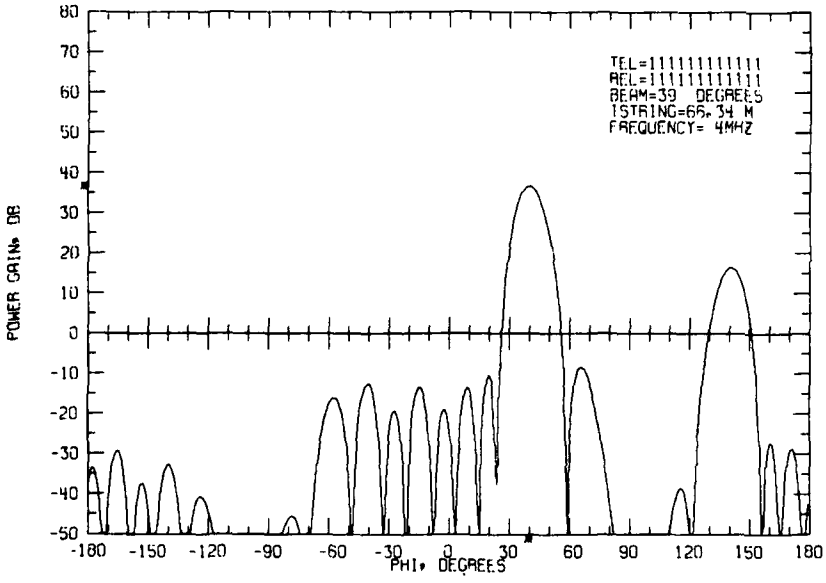

Fig. 3. Antenna pattern for 4 MHz operating frequency, mid string of three available in elevation, near zero elevation angle

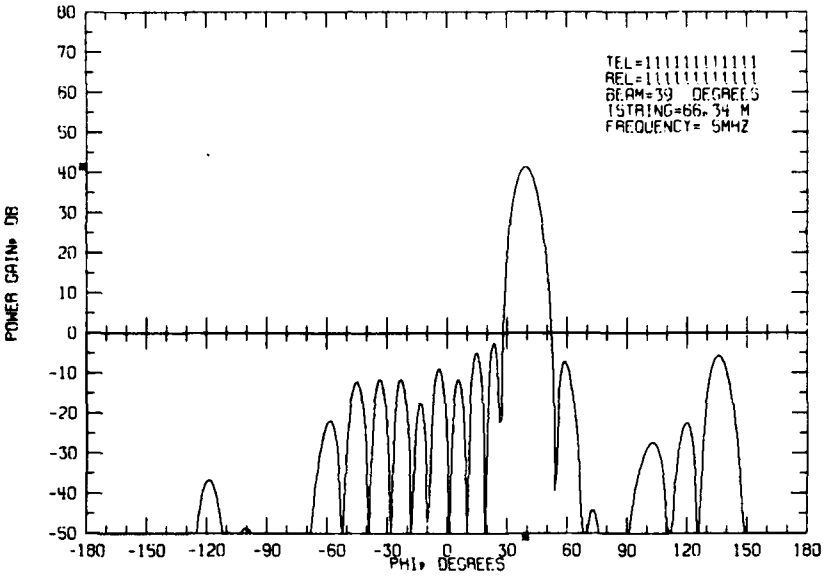

Fig. 4. Antenna pattern for 5 MHz operating frequency, mid string of three available in elevation, near zero elevation angle

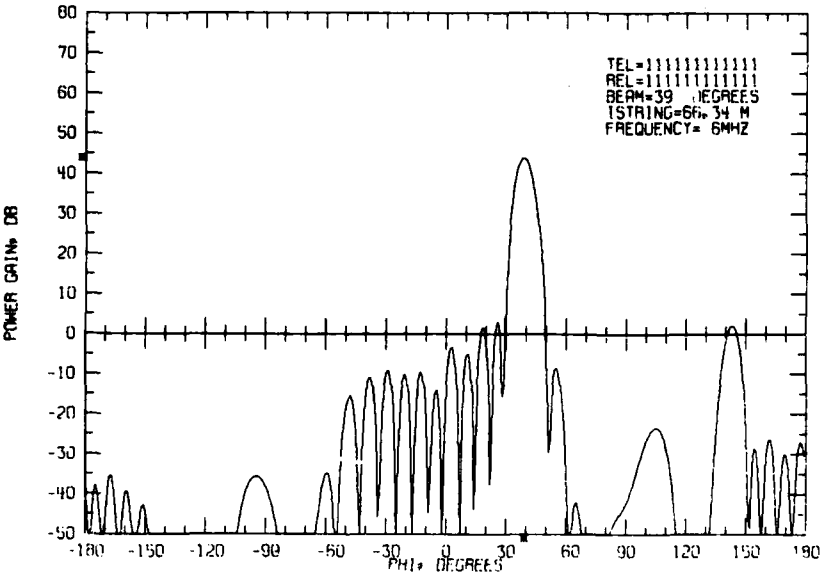

Fig. 5. Antenna pattern for 6 MHz operating frequency, mid string of three available in elevation, near zero elevation angle

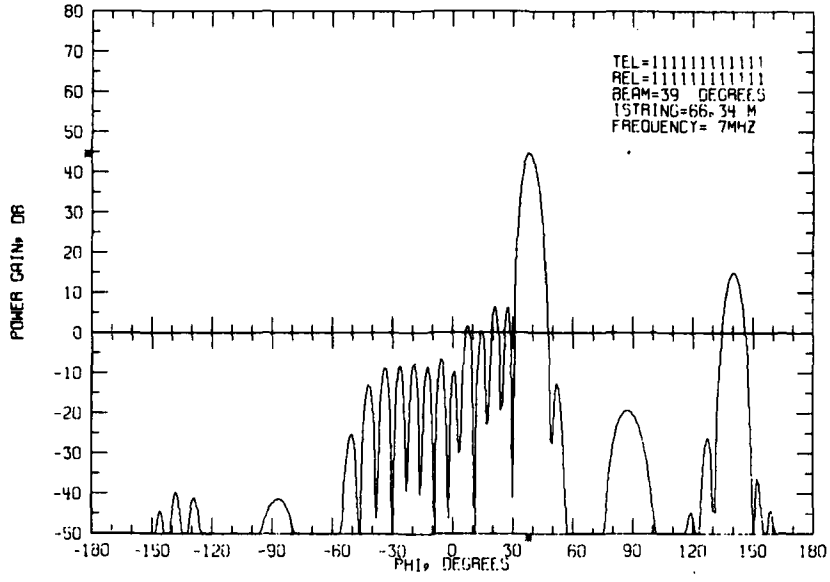

Fig. 6. Antenna pattern for 7 MHz operating frequency, mid string of three available in elevation, near zero elevation angle

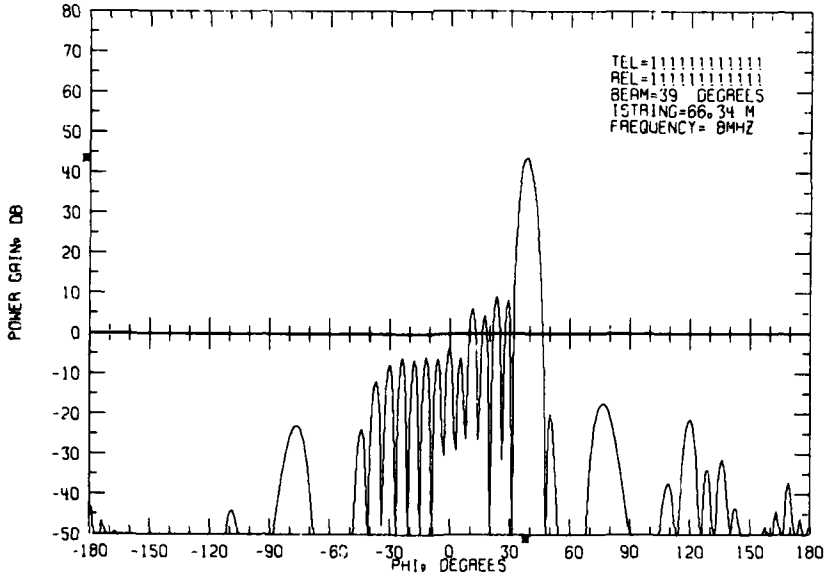

Fig. 7. Antenna pattern for 8 MHz operating frequency, mid string of three available in elevation, near zero elevation angle

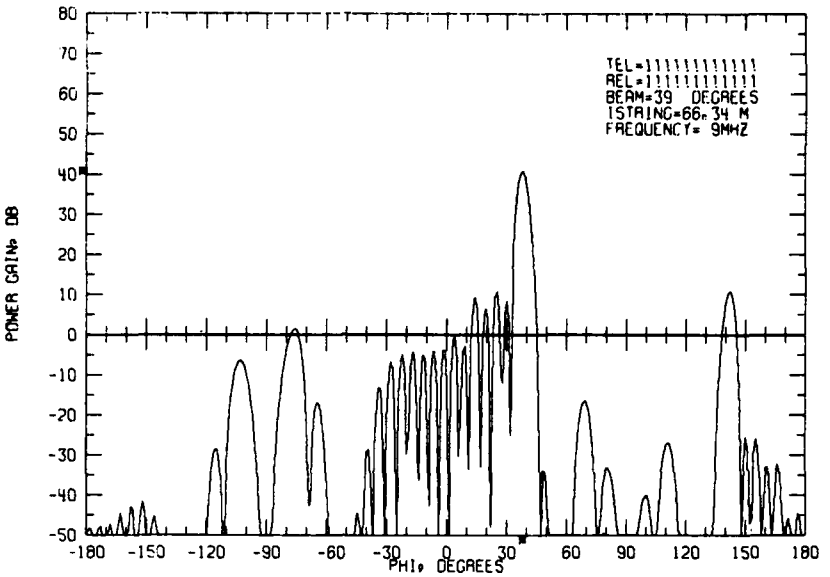

Fig. 8. Antenna pattern for 9 MHz operating frequency, mid string of three available in elevation, near zero elevation angle

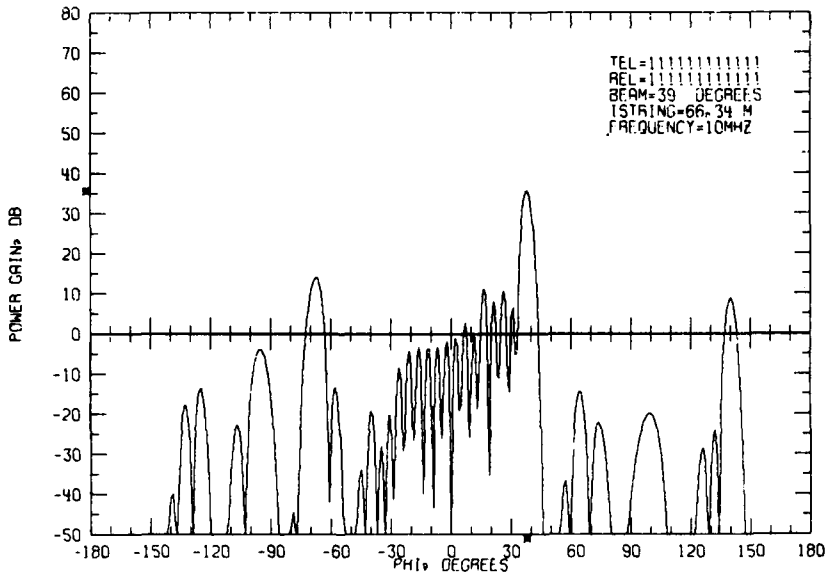

Fig. 9. Antenna pattern for 10 MHz operating frequency, mid string of three available in elevation, near zero elevation angle

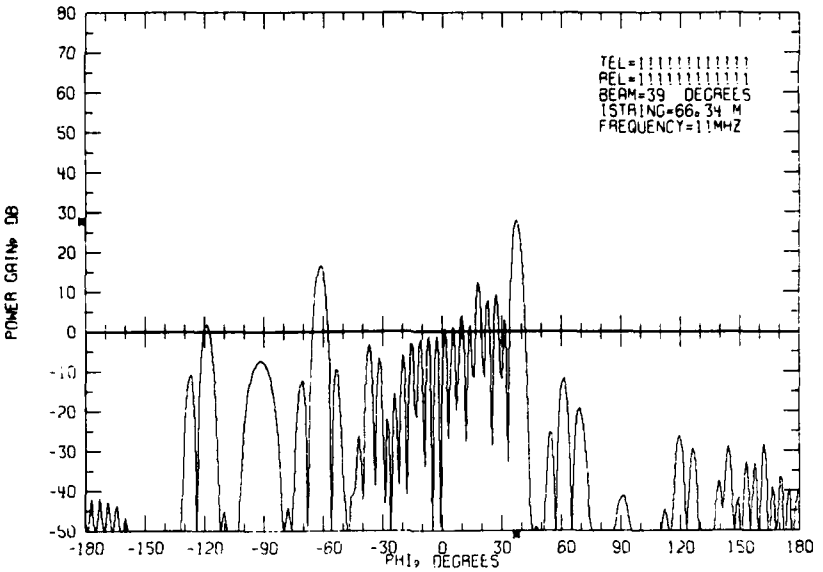

Fig. 10. Antenna pattern for 11 MHz operating frequency, mid string of three available in elevation, near zero elevation angle

A DESCRIPTION OF RADAR OPERATION AND DATA PROCESSING

The data reported upon were collected using the SEA ECHO radar located on San Clemente Island, Calif. It is unique in that it is the only HF radar known that is located at the edge of deep ocean waters with a high azimuthal resolution antenna that can operate in the surface wave mode to conduct oceanographic studies. The antenna has a 381-m aperture, 25 elements spatially tapered, which produces a two-way beamwidth of 2 deg at 15 MHz operating frequency. The beamwidth broadens inversely with radar frequency. The antenna can be phase steered in 2-deg steps, 40 deg either side of its boresight of 320 deg true bearing, in two different operating configurations. In the first, it is steered 20 deg either side of boresight on a pulse to pulse basis, giving simultaneous coverage from 300 to 340 deg true bearing. In the second mode, it is steered from 280 to 300 deg, then 320 to 360 deg, again on a pulse to pulse basis. For this experiment, data were typically collected in alternate fashion in each mode for 30-min periods. In the first mode, the radar can be operated from 2 to 25 MHz, with no degradation in sidelobes; in the second mode, the upper limit in operating frequency is of the order of 11.5 MHz at the most extreme viewing angles, where sidelobes are generated which curtail meaningful operation. The antenna has been described in greater detail in another publication, which can be referenced for more information [3].

In addition to scanning in angle, the radar can be made to scan in frequency on a pulse to pulse basis. The format allows a scan in frequency over a preselected list for the first azimuth selection, steps to the next azimuth and repeats the frequency scan, and so on through the set of preselected azimuths. The radar is currently limited to an operating pulse repetition frequency (PRF) of 200 pulses per second because of timing constraints on the frequency sweep.

Being a pulse-Doppler radar, the Doppler spectrum is determined by the PRF; only one receive channel is used so that the unambiguous Doppler spectrum is just one half the PRF. A useful PRF was determined in the following manner. For the highest operating frequency, 25 MHz, the Bragg lines in the radar spectrum appear roughly 0.5 Hz either side of the carrier frequency; for lower radar frequencies, the Bragg frequencies are less. Hence, 1 Hz either side of the carrier was chosen as sufficient to display all relevant sea scatter information, yielding a 2-Hz unambiguous spectrum, and, therefore, a 4-Hz PRF. Note that the local oscillator for the phase locked receive system is offset half the PRF, so that the carrier frequency appears in the middle of the Doppler spectrum. Hence any return from a stationary target, such as land, is returned at the carrier frequency, at 1 Hz in a 2-Hz Doppler spectrum, with a PRF of 4 Hz. With a typical 4-Hz PRF for one frequency at one azimuth (i.e., one channel), the total number of channels to which one is constrained by the 200-Hz system PRF is 50. This is the product of the number of radar frequencies times the number of azimuths one selects. Consideration of beamwidth broadening with frequency and the upper limit of 11.5 MHz for the outermost beams led to a choice of ten frequencies, spanning 2 to 11.5 MHz (0.14 to 0.35 Hz wave frequencies); and five beam positions, stepped at 8 deg, selected so that even stepping occurred over the total coverage of the antenna beginning at 285 deg true bearing.

The radar returns were sampled typically at a single range, 150 μs (22.5 km distance to patch center), although more range samples are possible. A Doppler spectrum for each channel is created in the following way. A sample of the backscattered radar energy is sampled at the desired range cell for a particular frequency and azimuth and is stored on magnetic tape for each phase coherent pulse transmitted four times per second. If the backscatter return were from a stationary target within the range cell, the IF signal which is sampled would vary sinusoidally with the 1-Hz frequency; since the scatter from the sea is much more complex than this, the time variation of the sampled IF is a complex function of time. This time history is stored on magnetic tape for the period of the test run, typically one half hour. The number of digital samples stored for this period would therefore be of the order of 7200. The digital samples are then read into a computer and a Fast Fourier Transform applied to the digital time history. Using a 1024 point transform results in a 256-s output power spectrum. With the unambiguous Doppler bandwidth of 2 Hz set by the 4-Hz Nyquist sampling rate, this results in a 15.625 mHz spectral resolution. If the only scatterer were the stationary one mentioned earlier, the power spectrum would consist of simply a single component at 1 Hz in the Doppler spectrum. The complex time history of the sea return produces a spectrum which consists of two first-order components in the Doppler spectrum, the Bragg lines, equally spaced either side of the carrier frequency at 1 Hz, as is shown in the example of Fig. 11. The velocity associated with these equal but opposite Doppler shifts is the phase velocity of the resonant ocean wave components that are responsible for first-order scatter, those with wavelengths one half the radar wavelength, which satisfy Equation (1). The Doppler component to the right of zero represents scatter from that component of the directional spectrum which is running parallel to the look of the radar, with an approach aspect. Similarly, the component to the left of zero in the Doppler radar spectrum is due to scatter from the same wavelength component, but in a direction receding from the radar. The phase velocity of the wave components is determined by the dispersion rule for linear gravity waves

$$\Omega^2 = gk\,, \tag{7}$$

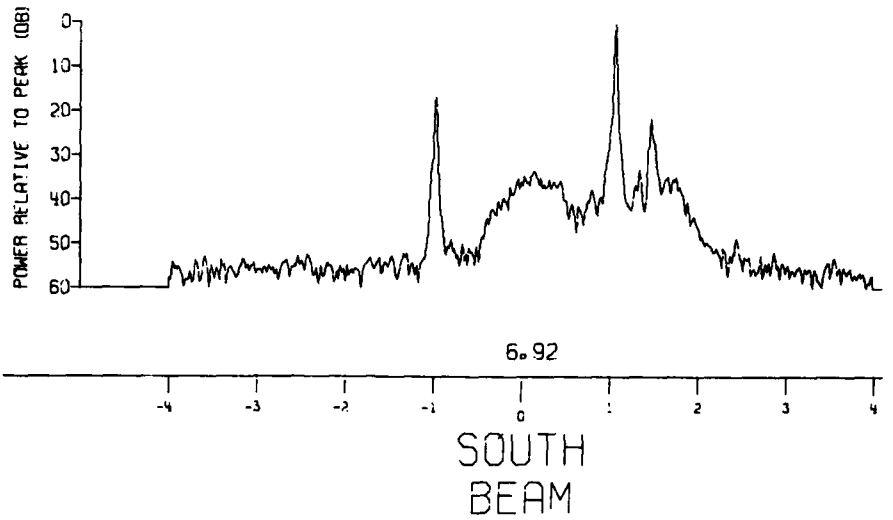

Fig. 11. A typical HF radar Doppler sea backscatter spectrum collected using a radar frequency of 6.92 MHz. Two narrow first-order returns occur at the Bragg frequencies, ± 0.268 Hz either side of the carrier frequency. The local oscillator has been shifted by 1 Hz relative to the carrier so that zero Doppler occurs at 1 Hz in the Doppler spectrum. The Doppler frequency axis has been normalized to the Bragg frequency, so that the first-order returns occur at ±1. The lower amplitude energy between the Bragg lines and to their right are second-order returns from longer wavelength ocean wave components than those responsible for the first-order returns, with wavelengths one half the radar wavelength. The directional spreading of the ocean wave spectrum presented in this report was determined by measurement of the amplitude of the strongest Bragg line as a function of radar look angle.

where Ω is the wave frequency, and g is the acceleration of gravity. The phase velocity of an ocean wave component is then

$$v_p = (g/K)^{1/2}, \tag{8}$$

which determines the Doppler shift of the two Bragg lines of Fig. 11. Shear currents have the effect of translating the entire Doppler spectrum by an amount determined by the radial component of that current.

A data set consisting of a half hour time record will produce roughly seven spectra, which are then averaged to produce the type of display shown in Fig. 11. Second-order features in the Doppler spectrum, which lay between the two first-order Bragg lines and outside of them, are due to second-order processes and contain information about the sea spectrum at wavelengths other than the Bragg wavelength, and at angles other than the look angle of the radar. These features have been investigated in other works and will not be further considered here [4-6].

The radar was run for these tests in a 50-channel mode as described above, using ten radar frequencies and five azimuthal positions for the outer and inner sets of azimuthal angles. Hence, 100 azimuthal-frequency values of the directional wave spectrum are determined for a 1 h data collection period of this type. The radar equation was then solved so that relative

values of the spreading function for different look angles could be calculated based upon relative measured values of received power and theoretical values of antenna gain. All other parameters in the radar equation are unchanged with changing look angle. These results were then used with values of the omnidirectional measurements made with the Waverider buoy to determine directional spectrum measurements via Equation (6).

WAVERIDER BUOY MEASUREMENT TECHNIQUE

A Datawell Waverider surface buoy was used to obtain omnidirectional wave spectra concurrent with radar operation. It was located at a point 16 km from the northern tip of San Clemente Island along the boresight bearing of the radar, 320 deg, anchored at a depth of more than 100 fathoms. The Waverider buoy transmits a signal with a frequency modulation which is proportional to its vertical acceleration. This signal was received at the radar site by a radio receiver (provided by Datawell) that demodulated the buoy signal, processed it, and produced a voltage variable in time which was proportional to the buoy oscillation amplitude in the vertical dimension due to the ocean wave structure. This signal was then low pass filtered and processed with a Ubiquitous spectrum analyzer with an effective integration time of 500 s and frequency resolution of 0.002 Hz. New data were read in each 50 s with the oldest 50-s portion at the front of the 500-s time record replaced by a new 50-s portion data string at the rear, then stored. This resulted in a time overlap factor of 10—that is, the output spectra of the Ubiquitous spectrum analyzer were completely decorrelated only after ten spectra were produced. The purpose of this was to smooth the averaged spectrum in the frequency domain. The series of spectra were then incoherently averaged over periods of anywhere from 1/2 hour to 4 hours, but typically 1 hour. The averaged data were plotted automatically in real time on an X-Y plotter, an example of which is shown in Fig. 12. The vertical scale is log amplitude. The horizontal scale is log frequency, so that the exponent of the falloff of the data can be easily determined, -5 for a Phillips asymptote. In the frequency domain, the Phillips asymptote in the saturated region of the spectrum is written:

$$S(\Omega) = \alpha g^2 \Omega^{-5}, \tag{9}$$

where α is sometimes referred to as Phillips' "constant" but which has been shown to be a fetch dependent quantity by Hasselmann et al. [7]; and g is the acceleration of gravity. On a per Hertz basis,

$$S(f) = 6.4 \times 10^{-4} \alpha g^2 f^{-5}. \tag{10}$$

The buoy spectrum shown in Figure 12 was collected on a day when the winds had blown for more than 36 h at speeds of 30 to 35 knots, sufficiently long to saturate the spectrum at the higher frequencies. The spectral components at just above 0.10 Hz and higher reflect these conditions in that they are driven to the saturation level. The components between 0.065 and 0.10 Hz are due to waves which have entered the area having been generated far at sea. They had been running long before the local spectrum had built up and are far down from the saturated values of their respective frequencies. Radar data were not collected during this period, but this spectrum is shown as an example of the only period for which fully saturated conditions were observed.

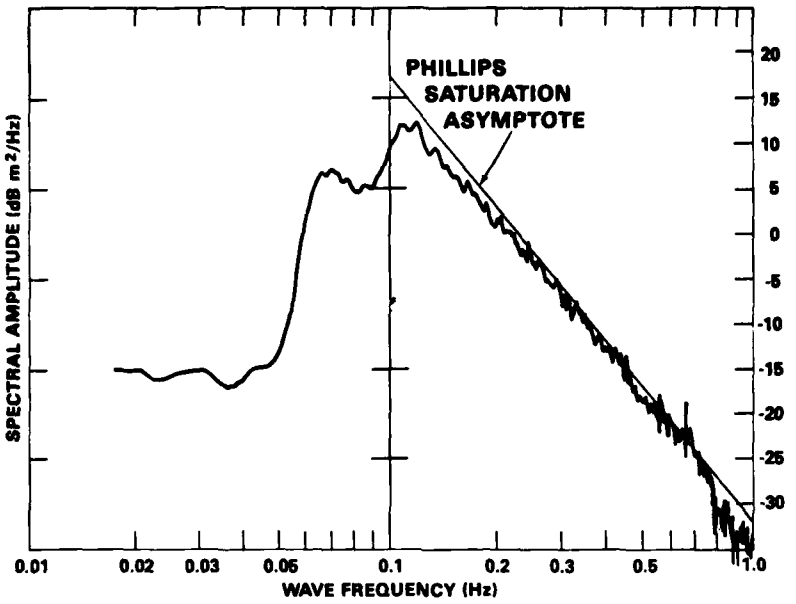

Fig. 12. An ocean wave omnidirectional spectrum measured by a Waverider buoy, averaged for a 1-h period. The spectrum is plotted on a log amplitude-log frequency basis to show the asymptotic behavior of the high-frequency portion of the spectrum. On this occasion the winds blew sufficiently long to generate a saturated spectrum, with high-frequency amplitudes driven to the saturation asymptote predicted by Phillips, which varies as frequency to the minus fifth power. The ocean wave frequencies sampled by the first-order Bragg radar scatter mechanism are equal to the Bragg frequencies themselves. In this report radar frequencies spanned 2 to 11.7 MHz, sampling ocean wave frequencies 0.144 to 0.349 Hz over 80 deg of viewing angle.

Normalization of the Spreading Function

As was stated earlier, the spreading function defined by Equation (6) is normalized such that its integration over all angles gives unity. In the data analysis which follows, we find it convenient to fit different models of the spreading function to the Bragg line amplitudes as a function of azimuth. It was found that for different times, different functional forms fit various sets of data, so that determination of the normalization constant for each of these was required for appropriate sets. The form of the fitting function that is used is:

$$F(\theta) = 10 \log((\gamma/\pi)\cos^{2N}\theta), \tag{11}$$

where γ is the normalization constant within a factor of pi. For $N = 0$, the simplest model, in which energy is distributed equally in two quadrants either side of the driving wind direction, the constant is unity. For $2N$ equal to 2, 4, 8, 16, and 32, the normalization constant is -3.0, -4.25, -5.63, -7.07, and -8.55 dB, respectively. It is to be noted that these constants have an impact on the determination of the value of the average scattering cross section of the sea. Barrick [2] used the $2N = 0$ model in his definition, in which he assumed the spreading function was constant with angle, and found σ^o to be -29 dB when measured by a surface wave radar for a fully developed Bragg wave component. (Note that he used a constant of 0.01 in

Equation (9).) Using this spreading function, if the radar were to scan in angle 90 deg either side of the wind direction, the same value of σ^o would be measured, −29 dB. A Waverider buoy would simultaneously measure an amplitude equal to the Phillips asymptote at the appropriate Bragg frequency. However, if the wave spectrum has some directionality to it, i.e., a value of $2N$ greater than zero, energy lost at angles off the wind direction in the directional wave spectrum must be compensated for by an increase in energy along the wind direction, so that the integrated value over all angles remains the same, the saturated value measured by the buoy. Therefore, the value of σ^o changes as well with an increase of 3 dB when measured in the direction parallel to the wind angle for a cosine squared spreading function, giving a value of −26 dB in this direction. Similarly, σ^o becomes −24.75, −23.37, −21.93, and −20.45 dB for spreading functions with cosine fourth, eighth, sixteenth, and thirty-second forms, respectively. These values then decrease with angle off the wind direction according to their respective spreading functions. Note that in each case the omnidirectional spectrum measured by a buoy would yield the same values. Hence, if one is to use the omnidirectional wave spectrum measured by a buoy as a calibration for σ^o, one must have some estimate of the spreading of energy with angle and adjust σ^o accordingly. This has been done in the data analysis which follows. The various spreading functions are plotted in Fig. 13, normalized so that integration over the forward half plane yields unity.

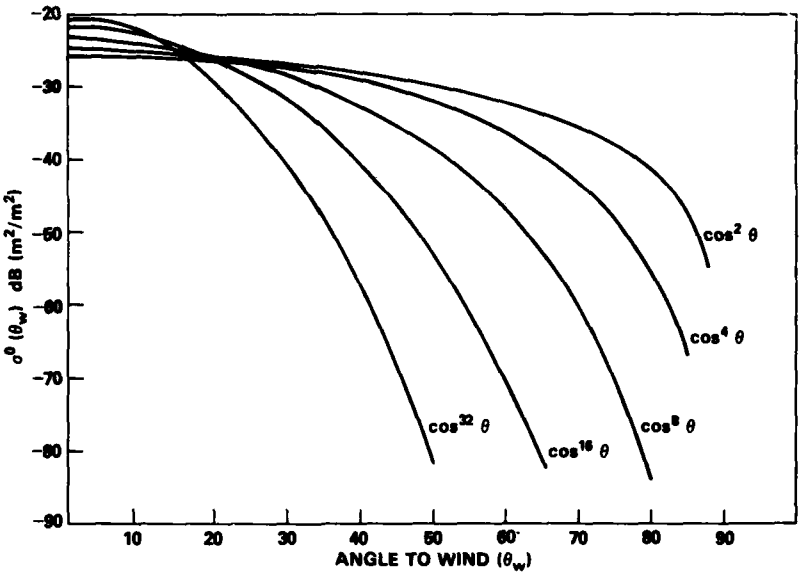

Fig. 13. Five different spreading functions, $F(\theta)$ defined in Equation (6), normalized to give the scattering cross section of the sea surface, $\sigma^0(\theta)$, via Equations (5) and (6)

A CASE STUDY FOR MARCH 31, 1977

The sea spectrum which prevailed on March 31, 1977, was an interesting one in that it contained a set of spectral components which probably represented a combination of three different wind wave systems: that due to local winds, which was observed to develop in the frequency spectrum with time; a broad band, lower frequency set of components which remained

relatively constant in character, suggested as due to a wind system which was reported some 200 miles west of San Clemente Island; and a very low frequency, narrow band component, quite often observed in previous Waverider buoy measurements near San Clemente Island in conjunction with other radar experiments. This last contribution to the spectrum is suggested as due to southern hemisphere generated swell, as observed at San Clemente Island by Munk et al. [8]. Ocean wave spectra for March 31, 1977, are shown in Fig. 14, the first of which was collected at 12:50 local Pacific time, the rest of the series covering roughly a 12-h period. The narrow band component at 0.45 Hz, which moves slowly to 0.50 Hz from the first spectrum to the last, is that suggested to be due to swell generated in the southern hemisphere. It has traveled sufficiently far for group velocity dispersion to act as a filter in the frequency domain, allowing the fastest and longest wavelength components to arrive first. These components are expected to be very narrow in their angular distribution as a result of the long distance propagated. The broader spectrum beginning at about 0.07 Hz is associated with a storm which was reported to be some 200 miles west of San Clemente Island, by Naval Fleet Numerical Weather Service reports especially provided for the southern California experiment. In contrast to the narrow band swell component, this energy is quite broad, extending to 1 Hz and beyond, where it aliases in frequency. The earliest waves spectrum of the set barely shows the effects of local winds at about 0.25 Hz, and is fit reasonably well by frequency to the -2.5 power. One might expect that this contribution would be generally broad in angular spread as characteristic of open ocean wave spectra.

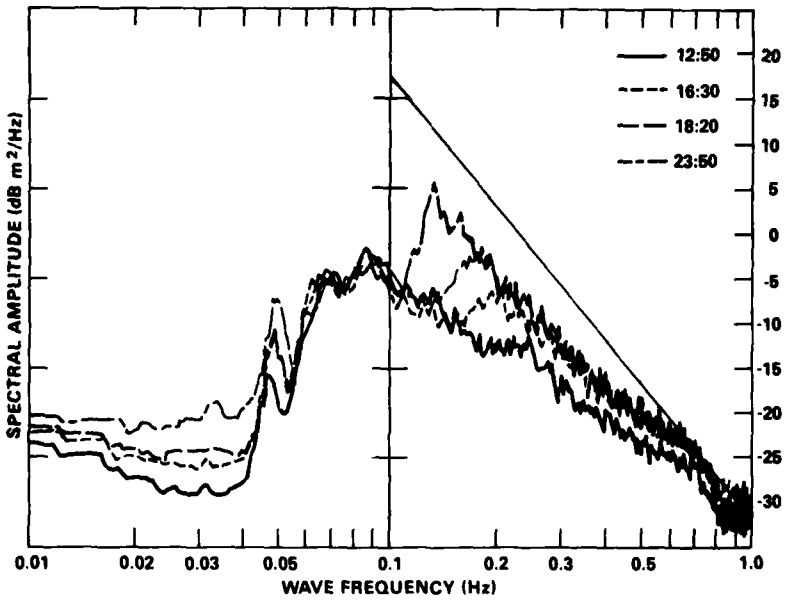

Fig. 14. Four different ocean wave spectra are plotted on a log-log scale for the times indicated, using a 2 mHz frequency resolution, and with each plot the result of 1-h incoherent averaging. Equation (7), with $\alpha = 0.008$, is plotted as a straight line. The broad band of wave energy from 0.06 Hz and higher is the result of energy which had propagated from the west from a storm at sea some 200 miles away. Wave energy at frequencies above 0.1 Hz which shows a changing character from one time period to the next is the result of local winds blowing from 310 to 320 deg bearing over the time periods indicated.

Local winds began to blow at San Clemente Island about 7:00 a.m. on that day, from a direction estimated to be very nearly from the boresight direction of the radar antenna, 320 deg. Data obtained after the fact from the Naval Weather Service Detachment at the National Climatic Center, Asheville, N.C., collected at the weather station on San Nicholas Island, were in close agreement, with the reported wind speeds ranging from 10 to 14 knots. At the radar site, winds were observed to decay about midnight, so that a 17-h period of sustained winds was experienced at the minimum. These winds generated an ocean wave spectrum (as measured by the Waverider buoy) which began to become noticeable in the spectrum collected at 12:50 local time, and which is seen rising in successive spectra in Fig. 14. The spectrum for the period in which the winds ceased to blow at the radar site shows the maximum development, with the lowest frequencies excited of the order of 0.14 Hz, that probed by the lowest radar frequency used, 2 MHz. Spectra collected during the night showed the same general character, with no lower frequencies excited. The midnight spectrum can then be considered a bimodal spectrum, in the sense that two different major ocean wave spectra with two different primary directions are superimposed upon one another to produce the observed spectrum. The wind-driven portion can be considered a transient one, in light of the results which follow, rather than a fully developed steady state typically reported by other works.

The radar was run on March 31 from 11:15 a.m. local time, through midnight, until 6:30 a.m. of April 1. Data collection formats were varied. The data reported here are of the ten frequency-ten azimuth format collected over the 80 deg of coverage of the radar, as described earlier, beginning at 285 deg true bearing, and ending at 357 deg. Data collection periods were continuous over periods ranging from one half to one hour. The radar data reported here covered three general periods: 13:00 to 14:00, 17:20 to 19:30, and 21:25 to 22:35, all local times on March 31, 1977. They represent the period when the effects of the local winds first became noticeable in the Waverider spectral output, a period intermediate during the development of the high-frequency portion of the spectrum, and the period just before the local winds ceased to blow. Radar data collected through the night beyond this period showed a deterioration in well-defined shape in angular spreading; in addition, the buoy spectra showed no further development, but remained unchanged in character throughout the night.

The results of the radar measurements are shown in Figs. 15 through 23. These are plots of the angular spreading function, $F(\theta)$ of Equation (6), log amplitude on an arbitrary scale, versus radar look angle or true bearing from the north end of San Clemente Island. They were derived from the measured radar Doppler spectrum amplitudes of the approach Bragg lines, each of which was an average of 8 to 14 spectra in time. The standard deviations in the Bragg line used averaged over all frequencies and bearings for the three time periods reported upon were 4.6, 3.9, and 4.0 dB, respectively. The recede Bragg lines were not measurable on a large fraction of the spectra due to noisy channels at some azimuths and so were not included in these data. On several occasions where they were observable over all azimuths for a given frequency, they had roughly the same value with changing azimuth. This is probably because of the relatively low, nonsaturated sea conditions which were observed. The recede Bragg lines in this case were probably the result of general background wave amplitudes which were isotropic with angle. Crombie et al. [9] have suggested that the recede Bragg line is probably generated by nonlinear wave-wave interactions and should be related to the amplitude of the approach Bragg component. For the low seas which prevailed on this occasion, the waves were probably not sufficiently aroused for these interactions to occur. Hence, the amplitudes which were observed for these cases were probably due to background isotropic low-level swell.

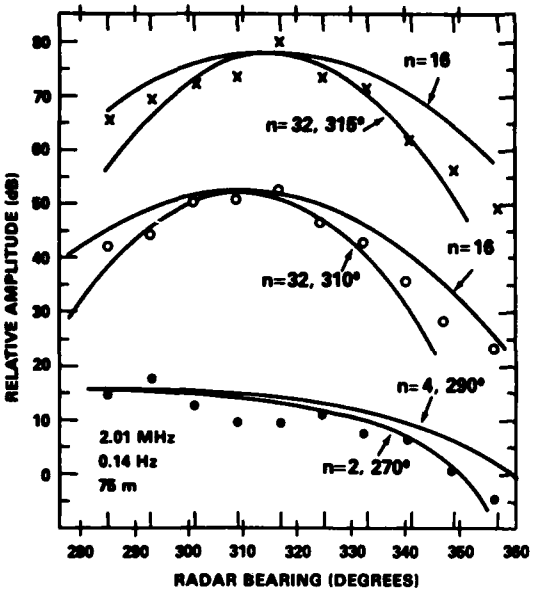

Fig. 15. Wave energy is plotted in log amplitude versus angle, on a relative amplitude basis, for three different time periods indicated in the text and in Table 1. The plots from one time period to the next are not related in amplitude. The straight lines are cosine to the n power curves drawn in for comparison purposes. In each case the power, n, and the peak angle of the curves are also given. The wave spreading with angle was derived from first-order Bragg line radar data nearly simultaneous in the time over angle and radar frequency, as described in the text. Ocean waves probed by the 2.01 MHz radar frequency were of 75 m wavelength and 0.149 Hz.

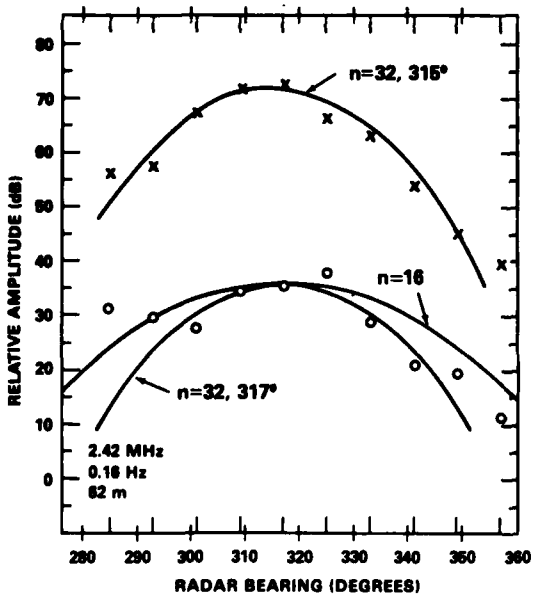

Fig. 16. The same as Fig. 15, but for only the second and third time periods, for 62-m waves and 0.16 Hz wave frequency

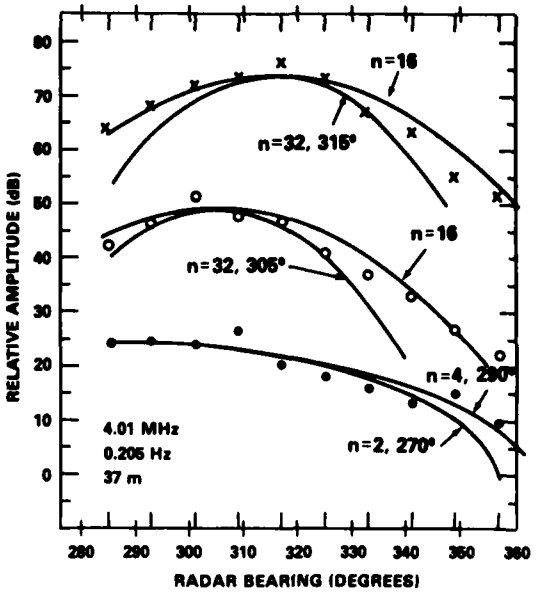

Fig. 17. The same as for Fig. 15, but for 37 m and 0.205 Hz waves

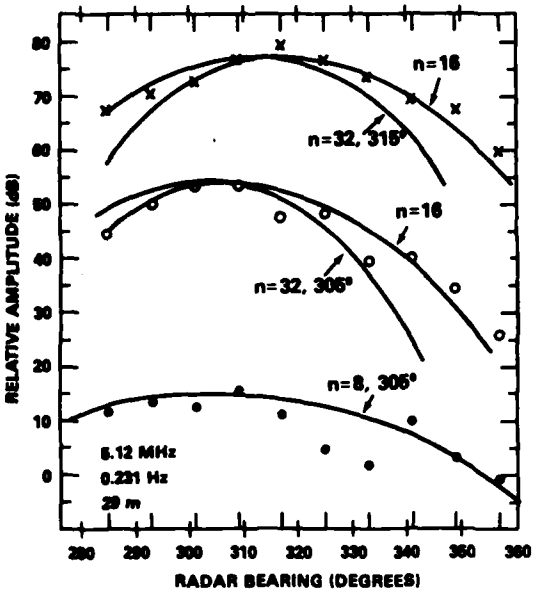

Fig. 18. The same as for Fig. 15, but for 29 m and 0.231 Hz waves

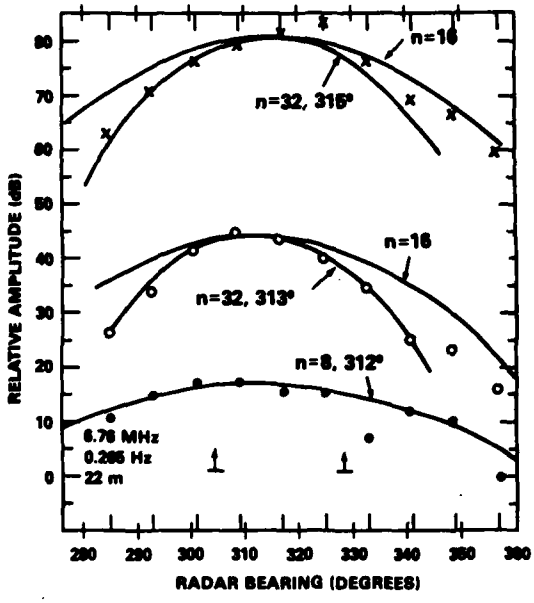

Fig. 19. The same as for Fig. 15, but for 22 m and 0.265 Hz waves

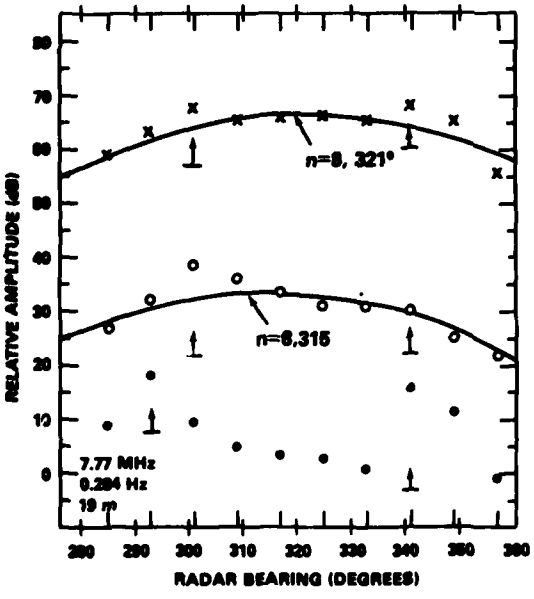

Fig. 20. The same as for Fig. 15, but for 19 m and 0.284 Hz waves

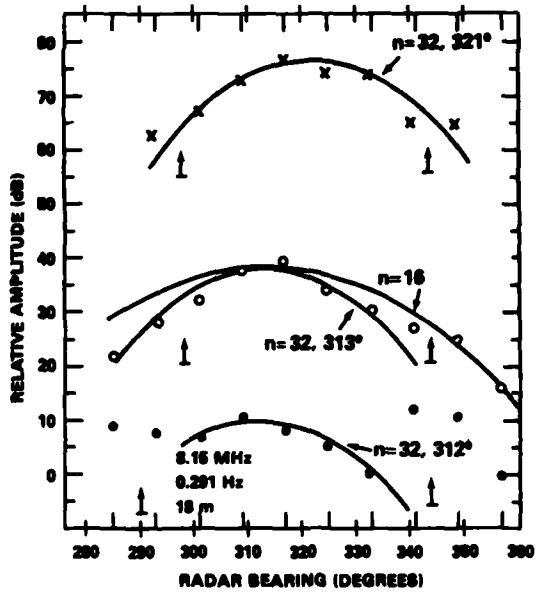

Fig. 21. The same as for Fig. 15, but for 18 m and 0.291 Hz waves

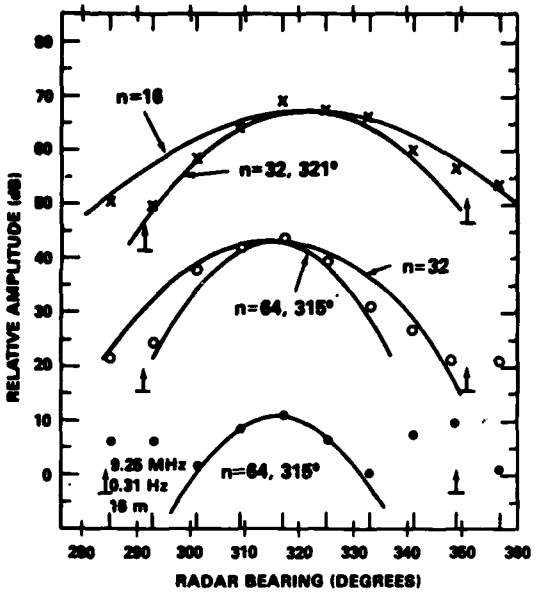

Fig. 22. The same as for Fig. 15, but for 16 m and 0.310 Hz waves

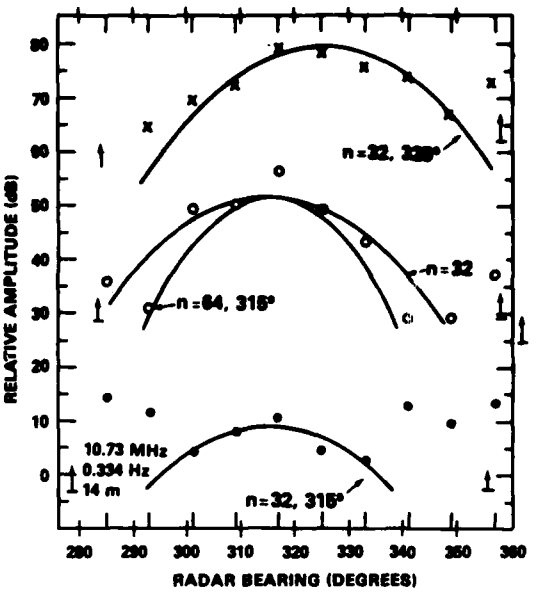

Fig. 23. The same as for Fig. 15, but for 14 m and 0.334 Hz waves

Each figure of three plots represents the three measurement periods defined above for a different radar frequency. The lowest plot of three represents the earliest time period. In the lower left corner of each figure is printed the radar frequency probing the sea surface, the wave frequency probed by the radar, and the wavelength of the Bragg ocean wave. The first of these figures shows results for the longest ocean wavelength probed, 75 m, by the lowest radar frequency used, 2.01 MHz. The lowest set of data points represents the spreading of wave energy for the time period 13:00 to 14:00 local time. At this time, these wave components should as yet be little affected by local winds, and should therefore show a shape in angular distribution associated with the system that created them, in this case, the storm far at sea which probably drove these components to saturation. Additional spreading may also be contributed by propagation effects. In any case the wave components show a fairly broad spread. Two possible fits are indicated, a cosine squared fit, centered about 270 deg, the direction reported at the time by a fleet numerical weather service report; the second fit, a cosine fourth, is centered at 290 deg, a direction reported by Scripps personnel operating a pressure sensor array north of the oceanographic research pier at the Scripps Institute for Oceanography, 90 miles east of the radar location on San Clemente Island. (Note that San Clemente Island lies due west of the Scripps array, so that they could not have measured a 270 deg bearing for these waves.) Neither fit is meant to be a definitive one, but only an indication that the spectrum was quite broad and centered about a direction other than that from which the wind was blowing. The scatter in the data is somewhat broad for a definitive fit to be made, as one might expect for a swell spectrum that has propagated some distance, roughly 200 miles in this case.

The second time period 75-m data (Fig. 15) show a narrow spread of ocean wave energy about an angle somewhere between 310 and 320 deg. Again, two curves have been fitted to the data, each centered about 310 deg bearing, cosine sixteenth and cosine thirty-second in functional form. The third period shows a similarly narrow spread, now about 315 deg. The same

two functions are fitted to the data as the second set. Hence, we observe in the transition from the first time frame to the second a development of a very narrow spread in wave energy due to local winds, in agreement with amplitude development reported by the buoy.

Figure 16 shows just the second and third of the three data sets for the 62-m waves probed by a 2.42 MHz radar frequency. The channel was too noisy to yield any data during the period the first set was collected. There is an asymmetry in the second time period, with an apparent contribution in the western direction from the Pacific swell. The data set for the third period shows less scatter about the fitted curve, although a slight contribution can still be observed from the western swell. The curves fitted to the data are again cosine to the n power, where n is sixteen and thirty-two. The directions are 317 and 315 deg bearing, respectively.

Figure 17 shows the spread of 37-m ocean waves resonant with the 4.01 MHz radar frequency. Again, the first data set shows little or no contribution from the local winds. The two curves fitted to the data are cosine squared about 270 deg bearing, and cosine fourth about 290 deg. These waves have not yet felt the effects of the local winds, and behave generally as the 75-m waves, with a similar spread and originating from a westerly direction. The second and third time frames again show the narrow spread observed for the previous two frequencies, and for similar directions, 305 and 315 deg, respectively.

The early time period for the next set (Fig. 18), the 29-m waves associated with the 5.12 MHz radar frequency, finally appear to show effects of local winds, as would be expected, since shortest waves are the first to respond to driving winds. A cosine eighth curve is fitted to these early data, centered about a 305 deg bearing. The following two time periods for this wave frequency show a similar spreading to the earlier frequencies with bearings of 305 and 315 deg for the second and third time periods, respectively. It is noted that the first time frame is in fact broader than the latter two, and noisier as well. This is probably due to the combination of swell and local effects determining the spread in a nearly equal manner, versus local winds alone determining the narrow spreads.

The 22-m waves measured by the 6.76 MHz radar frequency show (Fig. 19) a similar behavior as at 29 m, with the effects of local winds again contributing significantly in the first time period and shifting the primary wave direction relative to the swell, now to 312 deg, and again with a cosine eighth spread. The later two time periods again show the the cosine sixteenth and thirty-second behavior, about bearings of 313 and 315 deg, respectively.

At the 7.77 MHz radar frequency, the early time period shows (Fig. 20) a phenomenon much different from the longer wavelength responses. The 19-m waves show two sharp dominant peaks in wave growth, at 293 and 341 deg bearings, which we believe are generated by the winds from 315 deg in an early stage of wave growth. At the later time periods, the spread in wave energy also has a much different character than what was observed at the longer wavelengths, although still centered about a similar direction. The data are spread much more broadly in angle as is indicated by the cosine eighth fit for periods two and three, with primary angles of 315 and 321 deg. This is in contrast to the exponents 16 and 32 for the longer wavelengths. There are still slight maxima either side of the primary wave direction, now at 301 and 341 deg bearing. These angles are identified in Fig. 20 by vertical pointing arrows. We hypothesize that the energy peaks at these angles correspond to those associated with the Phillips resonance mechanism for wave generation by a turbulent wind field. This point shall be discussed further in a later section.

At 8.15 MHz, the data (Fig. 21) for the first time period for the 18-m waves are very similar to those for the last set, the 19-m waves. Vertical pointing arrows have been drawn in at angles predicted by the results for the 19-m waves. Maxima are indeed observed at these angles as predicted by the Phillips mechanism. The central region of angles appears to be fitted very well now by a cosine thirty-second fitted, centered about 312 deg bearing. Energy in this region is more developed relative to the resonance peaks as would be expected for a higher wave frequency. The later two time periods also fit reasonably well a cosine thirty-second curve, centered about 313 and 321 deg bearings, with energy in the windward direction now the dominant contribution. Arrows have again been drawn in at resonance bearings predicted by the results of the 19-m wave data set, and a slight rise from the fitting curve is seen in both cases as would be predicted by this mechanism.

Data for the 9.25 MHz radar frequency, the 16-m ocean waves (Fig. 22), behave very similarly to data for the 18-m waves (Fig. 21). Again, secondary maxima appear in the regions predicted by the results for the 19-m waves. The central region, however, is even narrower in angular spread, and the first two time periods appear to be best fitted by a cosine sixty-fourth curve, both centered about a 315 deg bearing. The suggested Phillips resonance contributions again appear at angles predicted by the 19-m results, more dominant in the earlier time period than the second, as would be expected by the nature of the mechanism. The last time period shows a spreading of wave energy to cosine thirty-second, with again some contributions at the resonant angle directions.

The data for the last two sets of wave frequencies behave again very similarly to the 18-m waves. Figure 23 shows Phillips resonance contributions near their predicted bearings, their amplitudes roughly equal in energy content to the windward wave energy, which peaks about the reported wind direction again, with cosine thirty-second spread. In the second time period, both data sets fit very nearly a cosine sixty-fourth spread, with again minor contributions from the Phillips resonance near their predicted angles. For the last time period the spectra have broadened somewhat in angle to cosine thirty-second, again with resonance contributions which are as yet reasonably strong in amplitude. Data for the tenth radar frequency are not presented because they were noisy in character and Bragg peaks could not always be measured. Those available data were similar in character to those depicted in Fig. 23.

The data are summarized in Table 1. The ten radar frequencies used, the Bragg related ocean wave frequencies, and wavelengths are listed in the first three columns, respectively. For each ocean wave component is indicated the exponent of the cosine fit to the data and the primary direction. The three time periods are indicated as A (13:00 to 14:00), B (17:20 to 19:30), and C (21:25 to 22:35). Several points become quite apparent when the data are reviewed in this condensed form. For the earliest time periods and longest wavelengths, which have not yet been strongly affected by the local winds, the angular spread is very broad near cosine squared, which compares reasonably with other measurements of directional wave spectral spreading. For early times the spreading due to local winds is generally much narrower than for later times. The behavior of the primary direction appears to shift with time as if in response to the passage of a front. The highest frequency components respond most quickly to the local winds and presumably represent the most recent winds. If this be the case, then a scan of the angles for frequencies of the first period of data indicates a directional slew, suggesting a shift of winds from a west-northwest direction to a more northerly direction. Angles for the second period show little change with time from the first period but show a similar slew of direction with frequency. Data for the last period show a northerly shift for all frequencies relative to the second

time period, and in more northerly a direction, in agreement with the conclusion drawn based on the data for a fixed time varying with frequency. The direction for the highest frequency now has shifted to north of northwest, and the directions for the lowest frequencies are similar to those for the high frequencies for the earlier time periods. Obviously, fetch effects are coming into play with energy probably transported at the group velocity into the scattering patch, having been generated outside the area at an earlier time. The data for 7.77 MHz show an especially broad spread relative to all other frequencies. The asterisk in the $2n$ column for this case indicates a fit was not made of the spreading because of the resonant features dominating. It is the frequency for which the bimodal structure is first observed and is the most dominant contribution to the wave growth. The broad spread is probably connected with the especially strong coupling of this wave generation mechanism at this frequency. This mechanism is now discussed in greater detail.

Table 1 — Results of the data analysis for the three time periods defined as A, B, and C. Column 1 identifies the radar frequency used. Column 2 lists the ocean wave frequency probed by Bragg scatter for the given radar frequency, while column 3 shows the corresponding ocean wavelength. The exponent, 2n, of the function, $\cos^{2n}\theta$, fit to the data are shown in the next three columns for the corresponding time periods. The last three columns list the direction of the peaks of the curves fit to the data for these periods.

f_R (MHz)	f_W (Hz)	L (m)	2n			θ_W		
			A	B	C	A	B	C
2.01	0.145	74.6	2-4	16-32	16-32	270/290	310	315
2.42	0.159	62.0	-	32	32	-	317	315
4.04	0.205	37.1	2-4	16-32	16-32	270-290	305	315
5.12	0.231	29.3	8	16-32	16-32	305	305	315
6.76	0.265	22.2	8	16-32	16-32	312	313	315
7.77	0.284	19.3	*	8	8	317	315	321
8.15	0.291	18.4	32	32	32	312	313	321
9.25	0.310	16.2	64	32-64	16-32	315	315	321
10.73	0.334	14.0	32	32-64	32	315	315	325
11.65	0.348	12.9	64	64	32	317	317	325

THE PHILLIPS RESONANCE MECHANISM FOR THE GENERATION OF WIND-DRIVEN WAVES

A brief review is given of the generation of waves by wind, in relation to the experiment at hand. In general oceanographers tend to characterize different wave growth mechanisms for purposes of comparison with theories by means of the time rate of growth of a given spectral component averaged over all angles, i.e., the omnidirectional value. This is so because most measurements of wave growth are generally made with omnidirectional measurement devices, such as the Waverider buoy used here. Not a great deal of attention has been paid to calculating the directional characteristics of the various wave generation mechanisms, probably also for this same reason. A counter example to this statement is found in the theory first proposed by Phillips for the generation of waves by the turbulence spectrum associated with a wind system.

This mechanism was later incorporated into a more comprehensive theory which included mechanisms dependent upon the average wind field. The directional dependence of the average wind contributions are aligned with the direction of the wind. Any spread in wave energy about the wind direction would be presumably due to wave-wave interactions or slight variations in the wind field which have not been deemed sufficiently interesting to consider.

The resonance mechanism is described by Phillips [10] and in some greater detail by Kinsman [11], as well as in the original work [12,13]. Basically, energy can be imparted to waves by wind either by pressure fluctuations in the wind field or by tangential stresses. By their very nature, tangential stresses cannot exist for a glassy smooth surface since the surface presents no friction to the average wind. Hence, one would expect the pressure fluctuation effects to be the first contribution to appear in the wave field. As the sea surface is excited, frictional forces can come into play and tangential stresses can now impart energy to the ocean wave spectrum. Phillips found it convenient to perform a Fourier analysis of both the turbulence spectrum being advected by the wind field, and of the sea surface, and to study the energy transfer for each Fourier component. The resonance concept comes into play when one considers that the most efficient energy transfer occurs when a Fourier component of the turbulence spectrum remains in phase for some extended period with the corresponding Fourier component of the ocean wave spectrum. The wave component moves with a phase velocity determined by the dispersion relation for gravity waves (which are important at HF radar frequencies; capillary waves must also be considered for much higher frequency radars) and is given by

$$C(K) = (g/K)^{1/2}, \tag{12}$$

where g is the acceleration of gravity, and K is the wave number for the ocean wave Fourier component. The turbulence spectrum is simply advected along at the average wind speed but has components at all directions relative to the wind direction. The longest ocean wave component that can receive energy from the turbulence spectrum is that for which the wind speed and the phase speed are equal. The direction of this ocean wave component in the directional spectrum will be along the wind direction. Longer wavelength components all travel faster than the average wind speed and cannot stay in phase with the appropriate turbulence component sufficiently long for the resonant interaction to occur. Shorter wavelength components travel slower than the wind speed and can interact at angles ϕ to the wind and satisfy the resonance condition,

$$U \cos \phi = C(K), \tag{13}$$

where U is the average wind speed. There are two directions defined by this equation, at $\pm \phi$ deg to either side of the wind direction. For shorter and shorter wavelengths, these angles tend evermore toward perpendicularity to the wind direction.

The amplitude of the ocean wave component generated by the resonance mechanism grows linearly with time, in contrast to the exponential growth with time of the Miles mechanism [10,11]. It is also proportional to the amplitude of the fluctuation spectrum of the turbulence power spectrum. Hence, for early times in the growth of the wave spectrum, the ocean wave amplitude-frequency spectrum should mirror the structure of the turbulence spectrum, until other wave growth mechanisms or nonlinear energy transfer mechanisms begin to dominate further development of the spectrum.

A second observable associated with the resonance mechanism, in addition to the resonance angle, is the time scale associated with the time period of coherence of the turbulent Fourier component. It is determined indirectly from a measurement of the angular bandwidth of the resonance line measured by the radar. If the turbulence component remained coherent with the wave surface for a very long time, the angular width of the resonance structure would be extremely narrow, a delta function as the coherence time tended toward infinity. Stewart and Manton [14] have calculated a spectral width associated with this coherence time and define it as the reciprocal of the coherence time times 2π. Hence, for a given angle α, there is associated a spread in frequencies, which they presume to be Gaussian in shape, given by

$$\delta(\Omega) = (\Delta\,\Omega\,\pi^{1/2})^{-1} \exp\left[-(\Omega/\Delta\Omega)^2\right], \tag{14}$$

where $\Delta\Omega$ is the suggested bandwidth. One could just as well have assumed a pole type resonance of the form

$$\delta(\Omega) = \pi^{-1/2}\,\Delta\Omega/(\Omega^2 + \Delta\Omega^2), \tag{15}$$

such that the bandwidth is defined as the 3 dB fullwidth of the resonance. In any case, this bandwidth is not measureable easily directly, but one can measure the corresponding bandwidth in angle. That is, for a fixed wave frequency and resonance angle, there will also be a spread in angle about the resonance angle derivable from the dispersion relation and the resonance angle formula in terms of frequency. Using the gravity wave dispersion relationship,

$$\Omega^2 = g\,K, \tag{16}$$

one gets

$$\cos\alpha = g/(U\Omega). \tag{17}$$

Taking the derivative of this equation and solving for the derivative of wave frequency with respect to resonance angle, one gets

$$d\Omega/d\alpha = \tan\alpha, \tag{18}$$

so that the full width at half maximum of the resonance in angle in terms of the coherence time, T, of the turbulence component is given by

$$d\alpha = 2\pi/(T\tan\alpha). \tag{19}$$

Intuitively, one can think of the bandwidth in angle as due to scatter from wave packets smaller than the radar cell, requiring a spectrum of frequencies of width, $\Delta\Omega$, to represent them. Because the turbulence component has a finite lifetime, and hence, finite scale size, it creates a wave packet which in this case is much smaller than the area over which the radar is averaging. The distribution of such wave packets can be considered to be a continuous one versus wave frequency, but because of the resonant nature of the Bragg scatter mechanism, those packets with central frequency just off the Bragg resonant frequency will be ever less effective a scatterer the further off resonance they are. Those wave packets off resonance by an amount $d\Omega$ will be observed at an angle slightly off the resonance angle by an amount $d\alpha$, with the relationship between $d\Omega$ and $d\alpha$ given by Equation (18). Appropriate expressions for the bandwidth in wave number space, dK, and scale size, dL, derived from Equation (17) and the gravity wave dispersion relation are given by

$$dK/K = 2\tan\alpha\; d\alpha \tag{20}$$

and

$$dL/L = (2\tan\alpha\; d\alpha)^{-1}. \tag{21}$$

The amplitude distribution of these wave packets should be exactly that of the turbulence, presumably a Komolgorov type spectrum. In principle, a measurement of turbulence over the radar cell simultaneous in time with a radar measurement could prove or disprove this conjecture.

In summary, in the early stages of development, the resonance mechanism generates wave components at the resonance angles determined by Equation (13). Wave components with K values

$$K \geqslant K_m = g/U^2 \tag{22}$$

are affected by this mechanism. For later times, energy is delivered to the wave system at angles aligned with the wind, and for K values less than and greater than K_m of Equation (22). Because of this predicted difference in angular distribution as a function of K, one might expect the omnidirectional spectrum to show evidence of this effect by, say, a change in slope with K at K_m. For K greater than K_m, the resonance and Miles mechanisms are at work, while for K less than K_m, just the Miles mechanisms are effective. This picture would hold only while wave-wave interactions are unimportant of course, before wave breaking becomes significant in the redistribution of wave energy with frequency and angle.

Phillips Resonance Parameters from Radar Data

From the March 31 observations provided by the Waverider buoy, an f^{-5} saturation asymptote was never reached for any wave component. Hence, one can assume that wave-wave interactions probably played little or no part in the development of the directional spreading of the measured directional ocean wave spectra. The hypothesis presented here is that the bimodal structure observed in the data as a function of azimuthal angle for wave components 19-m and shorter is due to the Phillips resonance mechanism. The 19-m waves show an especially strong bimodal feature, which is clearly the dominant structure in the earliest time period, some 15 dB stronger than the wave amplitude in the wind direction. The bimodal structure is the dominant contribution for the second and third time periods as well, and serves to present a much broader overall angular distribution than at any other frequency. Using Equation (10), one can measure the total angle between the twin peaks for 19-m wave data and calculate an average wind speed at which the turbulence spectrum is being advected. For the measured 48 deg spacing, and the wave phase velocity of 5.49 m s^{-1}, one gets a wind speed of 6.0 m s^{-1}, or 11.66 knots. For the second and third time periods, the left peak has shifted somewhat, yielding a wind speed of 5.84 m s^{-1}. Both peaks are clearly identifiable in each spectrum and are still the dominant features compared to the energy along the direction of the wind. This energy has grown in comparison to the earliest time period, as would be expected according to the theory discussed. The inferred wind direction from the peaks measured during the first time period is 317 deg; that of the second and third time periods, accounting for the shift of the left peak, is 321 deg. This agrees with the observation from Table 1 of a slow shift of wind direction from left to right, or, northwesterly to north.

Wave components with phase speeds greater than 6 m s^{-1} will not be excited by the Phillips mechanism and should not show the bimodal structure. The only spectrum with wave frequency less than 0.28 Hz which should show the Phillips resonance is the 0.27 Hz spectrum for the first measurement period, associated with the 6.76 MHz radar frequency. The plot of these data shows a peak at the appropriate bearing for the left peak, much broader than expected

compared to higher frequency observations, and a minor peak to the left of the predicted position for the right-hand peak. For later time periods, the phase velocity is greater than the calculated wind speed and no peak is expected. The results for the 6.76 MHz data should be considered marginal, at best, regarding the Phillips resonance.

One can estimate the fullwidths of the resonance features at half maximum, and determine the coherence times of the turbulence components discussed earlier. A pole-shaped curve was drawn over the two peaks of the 19-m data, as well as the right-hand peaks of the 18- and 16-m resonances. Fullwidths at half maximum for the 19-m radar data are 9.4 and 7.6 deg. For the 18- and 16-m data, the values are 11.8 and 14.1 deg, respectively. Values of dK/K from these widths are 0.146 and 0.118 for 19 m, 0.210 for 18 m, and 0.31 for 16 m. All are less than one, in agreement with the requirement of Stewart and Manton [14], a condition imposed in their derivation of the expression for the wave energy in a given direction to be independent of the turbulent time scale. The experimental results of Willmarth and Wooldridge [15] which they quote gave a value of 0.6 for dK/K. Our values are of the same order of magnitude and agree with the predictions of Stewart and Manton.

The turbulence coherence time scale determined from these angular widths are 86 and 106 s for the 19-m turbulence, 60 s for the 18-m component, and 40 s for 16 m. The scale sizes of the wave packets responsible for the radar scatter at the Phillips resonance angles are 163 and 132 m for the 19-m waves, and 87.6 and 57.3 m for the 18- and 16-m waves, respectively. The number of ocean wavelengths which are in resonance with a turbulence component are 8.5 and 6.8 for the pair of 19-m wave components, and 4.8 and 3.2 for the 18- and 16-m waves. This scale size of coherent patch size or ocean wave packet responsible for the radar scatter would also appear to be the scale size of the turbulence component, on the average, interacting with the ocean wave spectrum, if the turbulence spectral characteristics are indeed impressed upon the sea spectrum by the resonance mechanism as originally suggested by Phillips.

KITAIGORODSKY SCALING

An interesting calculation can be done relating the maximum expected wave spectrum that can be excited in the waters north of San Clemente Island by a wind blowing from the region of the Santa Barbara Channel Islands, a northwesterly direction. Kitaigorodsky calculated a relationship between the maximum frequency of the wave spectrum and the fetch available for wave generation, and is given by

$$\tilde{F} = 3.5 \times \tilde{X}^{-1/3}, \tag{23}$$

where $\tilde{F} = f\ U/g$ is a normalized frequency, and $\tilde{X} = x\ g/U$ is a normalized fetch, with U the wind speed measured at 10 m above the sea surface. Hasselmann et al. [7] have summarized their JONSWOP results along with ten other sets of data and verify the relationship over seven orders of magnitude of normalized fetch, running from 10^{-2} to 10^{5}. If one assumes that the fetch for a wind blowing from 315 to 320 deg bearing from the north end of San Clemente Island is determined by the Channel Islands, the fetch so defined is of the order of 150 km. The wind speed determining the Phillips resonance mechanism is taken to be at a height of one half the wavelength of the turbulence component, equal to the ocean wavelength being excited. For the radar frequency of 7.7 MHz, the ocean wavelength sensed is 19.3 m, so that the windspeed at half wavelength height is very near the 10-m height used in the Kitaigorodsky scaling equation. For a given fetch of 150 km and a wind speed of 10 m height of 6 m s^{-1}, the

normalized fetch and peak frequency are 4.08×10^4 and 0.105, respectively. This data point falls very nearly on the JONSWOP curve and yields a peak frequency of 0.172 Hz, just slightly higher than that observed in the Waverider buoy data. Note that for winds from the west, which normally prevail at San Clemente Island, the fetch is essentially unlimited, and fully developed seas should be observable.

DISCUSSION OF RESULTS

We have measured the angular spreading of a directional ocean wave spectrum which was bimodal in its angular distribution. That is, the measured spectrum was the result of two wave systems, one created some 200 miles west of San Clemente Island and which propagated into the area, while the second system was generated locally by winds from a northwesterly direction. The waves traveling from the west were probably fully developed when they were created, and their angular spreading was described quite well by a cosine squared distribution in angle, as has been reported before for fully developed waves. The locally generated waves were more transient in nature, showing a very narrow angular distribution about the wind direction. For those wave components with phase velocities less than the local winds, the Phillips resonance mechanism was suggested to explain the twin peaks in the spectrum, symmetric in angle about the wind direction, which varied with wave frequency as predicted by the mechanism. The wind speed which was derived from the position of the twin peaks in angle agreed well with that measured in the area by a weather station, both in regard to direction and speed. The twin peaks were found to dominate the angular distribution for the earliest measurement time period for 19.4-m waves, and were strong for the shorter wavelengths as well. For later time periods, wave energy aligned with the wind dominated the distribution at all frequencies, but remnants of the twin Phillips resonance peaks were still observable. This behavior is what one would expect for simultaneous measurements of several wave frequencies. The highest frequencies are expected to respond most quickly to winds and are indeed the first to show growth along the wind direction.

A measurement of the shape of the Phillips resonance peaks was made for three different wave frequencies for which the Phillips peaks stood sufficiently above other wave energy distributed in angle to allow a width to be determined. This was only possible for the earliest time period, as these peaks were dominated by wave energy along the wind direction for the later two time periods. Using the derivative of the equation relating the resonance angle to the phase velocity of a given wave component, one could relate the measured angle width at half maximum to the spectral width of the ocean wave packet. The scale sizes of the ocean wave packets ranged from 3.2 to 8.5 wavelengths, the smallest scale sizes associated with the highest frequencies. From the spectral width, the coherence time of the turbulence spectral component was calculated, following the work of Stewart and Manton. The assumption was made that the scale sizes of the ocean wave packets are determined by the scale sizes of the turbulence structure, following the statement by Phillips that, in the initial stages of development, the characteristics of the turbulence energy spectrum should be transferred to the ocean wave spectrum.

Details about the growth of wave amplitude with time from radar data were not readily available but should be retrievable from the recorded data not yet fully processed. Analysis of such data should allow one to identify growth rates of the various angular spectral components. One would expect the Phillips contributions to grow linearly with time, while the wave energy along the wind direction should exhibit an exponential growth with time. Such an analysis is planned in the future.

REVIEW OF PREVIOUS OCEAN WAVE DIRECTIONAL SPECTRUM MEASUREMENTS

It is worthwhile reviewing other directional spectrum measurement results in relation to the results reported here. In addition to using different measurement techniques, different environmental conditions were reported for each case. Hence, rather than the results of one method verifying another, the different measurements appear to give a broad view of the development of the directional spectrum, with the results reported here adding to that picture for periods early in the development of the spectrum.

The Measurements of Gilchrist

Gilchrist [16] has measured the angular variation of the direction of the Phillips resonance in an area with a fetch determined by the shore of an inlet near Vancouver. Because of the narrowness of the inlet, only one of the peaks was observed, while the other was damped by shallow waters and reflection effects. However, the existence of the Phillips peak in angle explained the variation in the peak of the directional spreading which was observed. The experiment did not have the dynamic range, i.e., the ability to detect a small value at one angle in the presence of a very large value at a second angle, that the HF radar has. This was due to the poorer angular bandwidth of the sampling array and the apparently poorer linearity of the array element instrumentation that was used. In the case of the HF radar, each sample in angle is an independent one, from a different patch of sea surface, and homogeneity is invoked over the total sampled area in deriving a directional spectrum. In the case of Gilchrist's measurements, the array is making a measurement in a single area, but the energy measured at one angle is affected by that impinging upon the array from a second angle, and bandwidth and dynamic range considerations must be taken into account in comparing energy from two different angles. Since the directional spreading was presented linearly in amplitude, rather than on a log basis, it is difficult to estimate bandwidth effects.

The Stereo Wave Observation Project

A second explicit measurement of the Phillips resonance is that of SWOP data by Cote et al. [17]. Directional spectra were measured by stereo pairs of photographs of the sea surface. Phillips [13] discussed these data in his paper, and they are discussed briefly in Kinsman's book [11]. Bimodal angular distributions were observed satisfying Equation (10) for ocean wavelengths from 44 to 73 m. Their character was similar to those observed here, with amplitude differences between the two peaks of the order of 3 dB. Samples appear to have been effectively taken every 5 deg with the stereographic processing. The spread with angle appears to be much broader than that observed here, but again it is difficult to determine angular bandwidth instrumentation and processing effects.

The Bomex Measurements of Regier and Davis Aboard FLIP

A very comprehensive set of directional measurements of ocean wave spectra is contained in the work of Regier and Davis [18] which is a condensation of the work reported in Regier's Ph.D. dissertation. The measurements were made using an array of wave sensors aboard the Scripp's oceanography vessel, FLIP, as part of the Barbados oceanographic and meteorological experiment (BOMEX). The environmental conditions were peculiar to the tropics and the associated meteorological regime, namely, many small-scale squalls distributed quasi-randomly

in space and time. Wind speeds ranged from 5 to 10 m s^{1} during the experiment. Saturation of the wave components was seldom observed. On 41 of the 42 wave spectra measured, a change in slope of the log amplitude-log frequency wave spectrum representation was observed in the region of three times the peak frequency, on the average. Below this cutoff frequency, the mean slope of the averaged nondimensionalized spectrum (normalized to the peak frequency) was -3.1; above the cutoff it was -4.3. None of the single spectra ever exhibited a -5 slope as predicted by Phillips. A second observation is that for all of the BOMEX observations, the phase speed of the peak frequency was roughly twice the local wind speed measured at 10 to 11 m above sea level aboard FLIP. The spectra were generally quite complex in directional spreading with frequency. In the two spectra represented in the paper [18] the energy peak in angle for a given frequency slowly changed with frequency, much like the angular slew reported here. In one case the change was a northerly one, in the second case it was a southerly one, both for easterly winds.

Fits to different functional forms for the spreading function were made: a $\cos^{S}\theta/2$ fit and a skewed exponential function were reported on [18]. Goodness of fit to the models was judged based upon correlation of the widths estimated for the spectrum with widths predicted by the functions. It was found that the two changed in a like manner, increasing and decreasing together, but the spectral estimate widths were greater than the predicted values. The best S value for the first model chosen appeared to be 4. They used simulated data with this functional form and compared it to the result averaged over all measurements incorporated into a normalized averaged spectrum. This corresponds to a $\cos\theta$ form over most of the forward half plane to within a decibel accuracy when compared with our data, a relatively broad result. They conclude that propagation of wave energy from other areas is important in their measurements, as evidenced by the variability of spreading with frequency, and the skewness of the spreading function (nonsymmetry) in angle for a fixed frequency. Under these circumstances, such a broad spreading function estimate is not surprising.

Finally, in a plot of RMS angular width versus normalized wave frequency $\hat{F}$ (normalized to the peak frequency, that of the highest amplitude component), the RMS width decreases with decreasing frequency. At a value of 3 the rate of decrease becomes more rapid, and more so again at a value of 2, until a minimum RMS width is reached at a value of 1. Beyond this the RMS width becomes broader again. In addition calculation of the correlation coefficient of the spectral density, $P(\hat{F})$, with wind speed was correlated at the 80% level or greater for $2 < \hat{F} < 3.5$, indicating a transfer of energy from the wind to waves is occurring in this frequency region. No comparisons were made with the Phillips resonance model to explain the variation of the RMS width with normalized frequency, or this correlation effect. We make the following observations regarding this possibility. The normalized frequency values, 2 and 3, were found to be, respectively, the values for which the wind speed equaled the phase speed of the wave, and the value for which a bend occurred in the slope of the omnidirectional spectrum; the frequencies between these values also show a high correlation of spectral density with wind speed. But the frequency at which the wave phase velocity equals the wind speed is just the one at which the resonance mechanism first begins to contribute, along the wind direction. For frequencies greater than this value, the mechanism continues delivering energy to the waves at ever-increasing angles to the wind direction. The resonance mechanism becoming operative at this frequency would account for the change in RMS width of the angular distribution of energy which occurs here, and the correlation discussed earlier also. At a value of normalized frequency equal to three, where a bend is observed, the rate of change of the RMS angular width

changes again, which may be evidence for yet another coupling of wind to waves, or perhaps the onset of a wave-wave interaction which redistributes energy within the spectrum as a function of frequency and angle.

One final comment is made that the wave energy measured π radians to the peak energy direction is typically just 16 dB down from the peak amplitude. This is a relatively small value compared to HF radar measurements, which give 24 to 30 dB as typical values. Perhaps this is again evidence of the existence of energy traveling into the area from distant wind systems.

Directional spectral plots were obtained from Regier's thesis for all 42 of the spectra which were reviewed for occurrences of bimodal structure similar to this work. In a majority of cases such structure was observed of the 42 records reported, but quite often at lower frequencies than the resonance cutoff frequency determined by the wind velocity. One would expect to see a spread in the bimodal peaks with increasing frequency, as observed here, and as predicted by Equation (13), but such structure was not immediately obvious. Since the spectra were averaged over periods from 2 to 6 hours, perhaps such structure was averaged out, since it was of a transient nature in our data.

The Wake Island Synthetic Array Radar Measurements of Tyler et al.

A second directional spectrum measurement of interest is the radar scatter experiment by Tyler et al. [19] using Loran transmissions at 1.95 MHz on Wake Island in the Pacific. Simultaneous measurements were also made with a tilt buoy for comparison, which measures waveheight and its first derivatives in orthogonal directions; the first two angular Fourier components of an expansion of the angular spread of the directional spectrum can be calculated from these measurements. For the radar results they report for two of the nine days of the experiment, the seas measured by the buoy stationed north of the island were driven to saturation for frequencies above 0.25 and 0.49 Hz, respectively, with a -5 slope above these values. At the Bragg wave frequency of 0.14 Hz, the spectral amplitude was 5 dB or so below saturation. The winds were reported to be relatively steady throughout the periods of interest so that the spectra probably satisfied time and fetch requirements one might associate with a fully developed directional spectrum. This is to be contrasted with the conditions for our experiment, in which the waves should be considered in an early development stage and relatively transient in character.

Their results indicate that the directional spectra generally also have a much broader spread than that reported here. They fitted the functional form $\cos^S\theta/2$ to their data, both on a linear amplitude basis, which tends to weight the energy near the peak relative to other angles more highly, as well as on a log amplitude basis, which takes into account the energy over all angles more evenly. They report a range of S values from 2.8 to 12.8 for the linear fittings, and from 3.4 to 9.4 using the log fit. Their results are somewhat narrower than that reported by Regier and Davis, although that work calculated only one S value for all data collected, and did not allow for a variation of S with frequency as is sure to occur. Hence, a comparison of S values is not really realistic except in a very general way. Over the range of angles which we report our data, the two functions $\cos^{4N}\theta/2$ and $\cos^N\theta$ are nearly equal when viewed on a log amplitude versus linear angle plot. Hence, our broadest exponents for the westerly swell which propagated into the test area compare with the narrower S values of Tyler et al., which is not surprising since they were probably generated under similar open ocean conditions.

Regarding the comparison made by Tyler et al., of radar derived values of the exponent, S, with those derived from the buoy measurements, a few statements are in order. Because just the first two Fourier expansion terms can be derived from the wave height and slope measurements made by the buoy, it cannot resolve wave components with a narrower spread than cosine fourth of theta over two, unless a more accurate representation is used to define the buoy filter response. In the original formalism developed by Longuet-Higgins et al. [20], for cases when the measured response of the spreading is much broader than the filter function of the buoy, any function to describe the filter mathematically which had a similar 3 dB filter width was satisfactory, since the first Fourier coefficient of the filter function was the most important. However, in cases when the measured response shape is of the order of, or just larger than the shape of the proposed filter function, in order to determine the excitation function to a reasonable degree of accuracy, one must determine as many Fourier coefficients of the filter function as one intends to use in the determination of the excitation function. This is because the Fourier coefficients calculated from the measured co-spectra are each in turn the product of the respective Fourier coefficient of the filter function times the Fourier coefficient of the excitation. To measure a very narrow excitation spectrum, one requires a large number of coefficients, since the narrowness is determined by the higher order Fourier components. In the analysis of pitch and roll buoys, the filter function is chosen to be a cosine fourth of theta over two, for mathematical finesse and because the halfwidth of this function is of the same order as that of the measured buoy response. This function has just three Fourier coefficients which are nonzero, however, so that excitation spectra with equal Fourier coefficients to third term but wildly different in higher order terms will be measured as identical by a filter which truly has a cosine fourth theta over two shape. Whether or not such a filter is physically realizable is not important for this discussion.

Consider now the case of a buoy with an angular filter with identical Fourier coefficients to third order and similar width as the cosine fourth, but more terms in its Fourier expansion. In principle, one could determine the excitation Fourier coefficients to the same order as were provided for the filter expansion, assuming one can measure the required higher order ocean surface derivatives with the buoy instrument. However, if the buoy angular filter has a similar width as the cosine fourth filter, the higher order coefficients must be small compared to the first three, otherwise the filter would be a much narrower one. Hence, if the nonzero coefficients of higher order are very small, noise then becomes a problem in the extraction of the higher order excitation Fourier coefficient from the coefficient calculated from the co-spectra measurement, because the error in the measured coefficient may be of the same order as the coefficient of the filter to this high order. It follows that the two input spectra with coefficients equal to third order but differing thereafter will not be well differentiated by this second filter either. Though no calculations are presented here, one can state generally that there is a limit to the narrowness of an excitation spectrum that one can measure relative to that of the buoy filter function, and the S value for the representation used for the excitation is of the order of that assumed for the buoy filter, certainly not larger.

For the data of November 13 of Tyler et al., the set of S values determined by the buoy showed a rather wide spread about four, near the limit per our earlier discussion. According to the technique of deriving a set of S values from such data, such a spread is an indication that the assumption of this cosine S of theta over two is a poor one. However, according to our discussion on the limit of applicability of this technique, S values of the order of four are in the range of where one would expect the accuracy of the technique to become poorer, even if the model assumed were a correct one. The fact that the radar derived values of S from the linear

data fit and the log fit showed a spread as well is an independent indication of a poor choice of fitting function, for if the data fit the function exactly, the same result of S would be gotten using either technique. For the data of November 15, the spread of S values determined by the buoy is smaller, but still clustered about four, near the buoy system limit. The spread in the radar derived values is also smaller, but still in the region of four. No error analysis was done to determine if another functional form fit the data better than that chosen. This of course is not necessary if there exists no theory which would explain, based on first principles, one functional form over another. In point of fact, the functional form chosen is a convenient one from the point of view of parameterization and allows comparisons to be made from one experiment to another, but should not be viewed as the "correct" model, because no theory for such a model has been suggested.

The buoy omnidirectional spectra generated for the two days reported upon have breaks in wave slope much like those reported by Regier and Davis. For the data of November 13, the high-frequency portion of the spectrum is saturated to the amplitude level indicated in our Figs. 2 and 12. Near 0.4 Hz a break in the slope occurs from -5 to -3.75, roughly. If the peak of the wind driven portion is taken to be just above the Bragg frequency, say near 0.15 Hz, the normalized "break frequency," as defined by Regier and Davis, is 2.67. For November 15, the seas are again saturated for high frequencies and a break occurs near 0.25 Hz. For an estimated peak frequency of 0.10 Hz, the normalized break frequency is 2.5, with a change in slope from -5 to -3.10. In either case, the Bragg related frequencies are very near saturation and wave-wave interactions would be expected to be playing a part in the redistribution of wave energy with angle.

One other statement is also made about the radar measurements themselves and the instrument used. All of the directional plots of the wave spectrum made have a maximum upwind/downwind ratio of the order of 20 dB as viewed in the plots, and 17 dB if one uses the value in the abstract for the constant which is derived from this ratio. Other measurements by HF radars of this value range from as much as 24 to 30 dB. This Wake Island measurement is different from most other HF radar measurements in that waves from the opposite side of the island than one is intending to measure may be contributing to the measurement. This difference is so in this case for two reasons. The first is the very small size of Wake Island, which allows scattered radar energy to be received with little or no attenuation from all directions. Secondly, the effective front to back ratio of any antenna on a good ground plane cannot be expected to be better than 20 dB. Hence, wave energy approaching the antenna from one direction and measured as approaching Bragg component will be measured as a recede Bragg component as it passes the island and is viewed from the opposite direction in the back lobe. This spectral contribution would be attenuated in the radar measurement only by the front to back ratio of the antenna gain, no better than 20 dB. In the case of the radar on San Clemente Island, the antenna is situated at the north end of the island, and the front to back ratio is enhanced by the surface wave propagation loss along the 20-mile length of the island to far greater than 20 dB. For skywave propagation this is not necessarily true and one must be careful in interpreting the radar spectra. In any case, for the near-zero propagation loss encountered at Wake Island, the front to back ratio would be expected to be no greater than the 20 dB observed in the approach-recede ratios of the measured Bragg lines. In either of the fitting schemes that were used to fit the data to the function of equation, the value in the rear direction probably contributed little. Their measured spectra which fit the functional form $\cos^S\theta/2$ are probably realistic for the open ocean, long fetch conditions which they encountered.

Directional Measurements from the JONSWAP Experiment

The JONSWAP experiment was instrumented with five pitch and roll buoys and a linear array for directional spectrum measurements [7]. However, only one of the buoys yielded reliable directional data throughout the entire experiment. In addition, the digital logging system of the linear array failed, so that data had to be retrieved from analog traces from each of the elements. This resulted in a reduction in sophistication of directional analysis. Only the mean wave direction and RMS directional spread were calculated. These could be gotten from just two sensors of the array and could be compared with similar results from the buoys.

Results were averaged over all data which satisfied ideal fetch limited wave generation criteria. The averaged directional spectral RMS width determined by the two-element array for frequencies near the spectral peak was 19 $\pm$5 deg, corresponding to a pitch and roll beam width of 27 $\pm$ 8 deg. That expected for a cosine squared theta distribution is 31 deg. Hence, the narrower result implies an equivalent S value slightly greater than 4 for the $\cos^S\theta/2$ distribution. The result is still broader than that observed in our data.

A feature similar to that observed by Regier and Davis was also reported in the JONSWAP data. In a plot of RMS angular spread versus normalized frequency, the spread was found to be a minimum at a value of one, the peak frequency. In two of the three plots shown, a change in slope of increase of the RMS spread was indicated at a frequency of just less than two. No statement was made as to the cause for such a change in relation to any wave generation mechanism, however, the analysis of directional spreading appears to be a minor facet of the JONSWAP experiment, probably due to the instrumentation difficulties encountered. The primary reason for doing the RMS spread determination appears to be to identify an average spreading function for use in the calculations of energy balance in the variable fetch studies that were done. The assumption appears to have been made that the angular spreading was constant with fetch and that a cosine squared theta distribution was satisfactory. In light of the experimental difficulties encountered, not much more could be done at the time. Such an assumption may not be a physically reasonable one in general, however, although their energy balance calculations appeared to be insensitive to the distribution assumed according to the analysis they performed.

Cloverleaf Buoy Measurements by J. A. Ewing in the North Atlantic

J. A. Ewing [21] employed a cloverleaf buoy to measure directional spectra in the North Atlantic. This buoy is an improvement upon the pitch and roll buoy in that, in addition to measuring waveheight and its first derivatives, the wave slopes, it also measures the second derivatives, the wave curvature in two orthogonal directions. Hence, nine coefficients of a sine-cosine expansion can be determined, allowing expansion to 4θ. The choice of weighting used in analysis gives a filter function proportional to $\cos^8\theta/2$, which requires 4θ terms in its own expansion. This filter function has an RMS width of $\pm$ 29 deg. The wave conditions were similar to our observations, except under open ocean. Winds of up to 30 knots 2 days before the measurements at a distance of 750 km produced attenuated swell, which was then superceded by waves due to local winds of up to 17 knots. For wave frequencies 0.2 Hz and above, the seas became saturated to the Phillips' asymptote due to local winds. Amplitude plots for lower frequencies were not presented. Five sets of directional spreading were presented for swell conditions preceding the strong local seas, and five sets during the growth of local seas.

No statement as to the averaging time for a given record or the period between records was made, however. The function, $\cos^{2S}\theta/2$, was fit to the swell data and fairly narrow spectra resulted, compared to the work reviewed thus far. Values of S ranged from 15 at 0.1 Hz to 2 at 0.2 Hz. These high values of S appear to be larger than the S value associated with the filter shape of the buoy, and their validity is questioned based on our earlier discussion. Hence, nothing more can be said for these wind-driven spectra other than several of them may have exceeded in narrowness the filter function of the cloverleaf buoy.

In the plot of S versus wave frequency for the swell data, the spreading exponent changes in a linear fashion with frequency, much like the RMS spread did in Regier and Davis' work, although the two are certainly not equivalent. The significant thing to note, however, is that again a change in slope occurs with frequency. The change occurs at a normalized frequency of just less than two. In this case, however, propagation dispersion effects are coming into play in the variation of spread with frequency and wave generation effects and wave-wave interactions cannot be separated from these as a sole cause of the change in slope of the spread with frequency.

About all that can be said then regarding the narrowness of the spread of wind-driven waves measured by Ewing when compared to our work is that spectral narrowness was observed of the order of his instrument resolution, and therefore could have in fact been narrower. Because the wind-driven waves were driven to saturation over a large portion of the frequencies measured, wave-wave interactions could also have played a part in development of the angular spread. This is in contrast to our measurements, in which the wind-driven waves were down significantly from Phillips' saturation asymptote.

Cloverleaf Buoy Measurements by Mitsuyasu et al.

An analysis of cloverleaf buoy data collected off the coast of Japan has been performed by Mitsuyasu et al. [22]. One point of interest in light of the data comparisons being made here is that they show analyses of directional spectra using coefficients determined from wave height and wave slope measurements, the equivalent of a pitch and roll buoy, and compare these with analyses using the additional coefficients determined from wave curvature, which the cloverleaf buoy can recover. It is the equivalent of comparing a measurement using a filter function of the form cosine fourth versus cosine sixteenth of theta over two. As mentioned earlier, the cloverleaf buoy has a 3 dB beamwidth equivalent well approximated by a cosine sixteenth theta over two spectral shape, so that directional distributions broader than this can be well determined by this instrument, as compared to the cosine fourth theta over two limit of the pitch and roll buoy. Mitsuyasu shows one example in which he calculates S_j values in the same manner as did Tyler et al., and uses the $j = 1$ and $j = 2$ values as an indication of the spreading. In addition, if these two values are nearly equal, the model assumption of a cosine to the S power of theta over two is a good one for the directional distribution of the energy spectrum. In one set of data, Mitsuyasu measures S_1 and S_2 values as high as twelve at frequencies near the spectral peak, and the two values are in fact very nearly equal over virtually all wave frequencies that were measured, so that the assumed model is not a bad one. (Note that no error analysis was done determining goodness of fit to such a model as a function of how nearly equal the two S values must be.) For a second set of data, however, he determines values of $S_1 = 33$ and $S_2 = 26$, both of which indicate a spectrum much narrower than the buoy's response function. We believe such results only to the extent that they are an indication of the

wave spectrum being much narrower than the buoy response, but not necessarily correct values. To attempt an estimate of widths of spectra narrower than the response of the measurement device, one must represent the shape of the device response very accurately, rather than just by an arbitrary function which has nearly the same beamwidth as the device, since the retrieval of wave spectral information from the measurement involves the unfolding of the spectral response of the device from the measurement, as was discussed earlier.

Notwithstanding, the overall results are very interesting in that they show similar behavior to other experiments which we have discussed. The spreading is a minimum near the spectral peak. Changes in slope are difficult to detect, however, because of the poorer frequency resolution than that of the earlier work. If such a slope change did occur in the data, Mitsuyasu et al. did not attempt to calculate it. Using five different sets of data, they calculated values of S_1 and S_2 for each of several different wave frequencies and plotted the mean S value as a function of normalized wave frequency, $\hat{F}$, normalized in this case to the wave frequency whose phase velocity is equal to the wind speed:

$$F_W = U/C \tag{24}$$

and found a functional relationship. Most of the S values were less than sixteen, the S value of the buoy response function, so that their use in such an analysis is valid, in relation to our earlier discussion. They found the following relationship to hold:

$$S = 11.5\ \hat{F}^{-2.5} \tag{25}$$

up to the peak frequency of the spectrum, and then a precipitous decline for lower frequencies, following a form:

$$S = 11.5\ \tilde{F}_M^{-7.5}\ \hat{F}^5 . \tag{26}$$

The peak frequency of the different sets of data were near the value of one, but fell on both sides of one. That is, the frequency of the peak in the energy spectrum occurred at a frequency whose phase velocity traveled both faster and slower than the wind speed for different sets of data. Hence, different wave generation mechanisms were probably at work on the different occasions. This is in contrast to the work of Regier and Davis, for example, who found the peak frequency to be twice this normalization frequency in most of their data. Since the peak frequency is also a function of fetch, according to the scaling of Kitaigorodsky, the implication is that for a fixed normalized wave frequency, the spreading of wave energy is independent of fetch as well. Other than the derivation of this idealized form of spreading with frequency, no other results relative to our own data were significant. Suffice it to say that spectra were measured on one occasion which were narrower than cosine sixteenth of theta over two, and on other occasions had S values of sixteen, ten, and seven. No analysis relative to the cause of the spreading was done, for example, comparing the spread of energy with the Phillips mechanism or wave-wave interactions.

Discussion of Previous Measurements

In conclusion, one can make the following statements regarding the measurements of the directional spreading function which have been reviewed here, and which represent the most recent measurements under open ocean conditions. Virtually all of the measurements have been under steady state conditions, as opposed to the transient, early period wave generation which we observed. Some hint of the Phillips resonance contribution to the observed spreading

may be claimed for some of the measurements, but because of long period averaging, the Phillips mechanism could not be expected to be a very significant contribution relative to other mechanisms which prevail under steady state conditions. Tyler et al. did some rough calculations regarding invoking the resonance mechanism for order of magnitude estimates of wave spreading widths which involved some relatively broad assumptions. None of the other authors made any comment as to the possible cause of the spreading which they observed. None of the experiments observed spectral spreading as narrow as ours, nor the bimodal structure associated with the Phillips resonance mechanism. This is in part due to the relatively poor angular resolution of the instruments involved relative to our own. The synthetic aperture radio scatter measurements by Tyler et al. had better resolution than our own for the same wave frequency but did not observe very narrow spectra, probably because of the open ocean and long fetch conditions which were associated with their measurements. In summary, our work appears to be the only one in the literature which has observed the Phillips resonance mechanism at work in the generation of directional wave spectra, with the angular resolution necessary to unambiguously define the twin peaks in angle predicted by the theory.

REFERENCES

1. D.C. Crombie, *Nature* **175**, 681-682 (1955).
2. D.E. Barrick, *IEEE Trans.* **AP-20**, 2-10 (1972).
3. M.T. Ma and L.H. Tveten, *IEEE Trans.* **AP-24**, 340-347 (1976).
4. D.B. Trizna, J.C. Moore, J.M. Headrick, and R.W. Bogle, *IEEE Trans.* **AP-25**, 4-11 (1977).
5. D.E. Barrick, *Bound. Lay. Met.* **13**, 23-43 (1978).
6. B. Lipa, *J. Geophys. Res.* **83** (c2), 959-962 (1978).
7. K. Hasselman, T.P. Barnett, E. Bouws, H. Carlson, D.E. Cartwright, K. Enke, J.A. Ewing, H. Gienapp, D.E. Hasselman, P. Kruseman, A. Meerburg, P. Muller, D.J. Olbers, K. Richter, W. Sell, and H. Walden, in *Measurements of Wind-Wave Growth and Swell Decay During the Joint North Sea Wave Project (JONSWOP)* (Deutsches Hydrographisches Institute, Hamburg, 1973).
8. W.H. Munk, G.R. Miller, F.E. Snodgrass, and N.F. Barber, *Philos. Trans. R. Soc. London, Ser. A* **255** 505-584 (1963).
9. D.D. Crombie, K. Hasselman, and W. Sell, *Bound. Lay. Met.* **13**, 45-54 (1978).
10. O.M. Phillips, *The Dynamics of the Upper Ocean*, 2nd ed. (Cambridge University Press, London, 1977).
11. B. Kinsman, *Wind Waves: Their Generation and Propagation on the Ocean Surface* (Prentice-Hall, Englewood Cliffs, N.J., 1965).
12. O.M. Phillips, *J. Fluid Mech.* **2**, 417-449 (1957).
13. O.M. Phillips, *J. Mar. Res.* **16**, 231-245 (1958).
14. R.W. Stewart and M.J. Manton, *Geophys. Fluid Dyn.* **2**, 263-272 (1971).
15. W.W. Willmarth and C.E. Wooldridge, *J. Fluid Mech.* **14**, 187-210 (1962).
16. A.W.R. Gilchrist, *J. Fluid Mech.* **25** (4), 795-816 (1966).
17. L.J. Cote, J.O. Davis, W. Marks, R.J. McGough, E. Mehr, W.J. Pierson, Jr., J.F. Ropek, O. Stephenson, and R.C. Vetter, *Met. Papers* **2** (6) (1960).
18. L.A. Regier and R.E. Davis, *J. Mar. Res.* **35**, 433-451 (1977).
19. G.L. Tyler, C.C. Teague, R.H. Stewart, A.M. Peterson, W.H. Munk, and J.W. Joy, *Deep Sea Res.* **21**, 989-1016 (1974).
20. M.S. Longuet-Higgins, D.E. Cartwright, and N.D. Smith, *Ocean Wave Spectra—Proceedings of the Conference* (Prentice-Hall, Englewood Cliffs, N.J., 1963), pp. 111-131.

21. *J.A. Ewing, J. Mar. Res.* 27, 163-171 (1969).
22. H. Mitsuyasu, F. Tasai, T. Suhara, S. Mizuno, M. Ohkusu, T. Honda, and K. Rikiishi, *J. Phys. Oceanog.* 5, 750-760 (1975).